JOURNAL OF PETROLOGY | VOLUME 47 | NUMBER 10 | PAGE 2047–2071 | 2006 | doi:10.1093/petrology/egl036

Calculated Phase Relations in the System Na_2O–CaO–K_2O–FeO–MgO–Al_2O_3–SiO_2–H_2O with Applications to UHP Eclogites and Whiteschists

JIAN-JUN YANG[1]* AND ROGER POWELL[2]

[1]STATE KEY LABORATORY OF LITHOSPHERIC EVOLUTION, INSTITUTE OF GEOLOGY AND GEOPHYSICS, CHINESE ACADEMY OF SCIENCES, P.O. BOX 9825, BEITUCHENG XILU 19, BEIJING 100029, P.R. CHINA

[2]SCHOOL OF EARTH SCIENCES, THE UNIVERSITY OF MELBOURNE, PARKVILLE, VIC. 3010, AUSTRALIA

RECEIVED AUGUST 15, 2005; ACCEPTED JUNE 14, 2006; ADVANCE ACCESS PUBLICATION JULY 19, 2006

Pressure–temperature grids in the system Na_2O–CaO–K_2O–FeO–MgO–Al_2O_3–SiO_2–H_2O and its subsystems have been calculated in the range 15–45 kbar and 550–900°C, using an internally consistent thermodynamic dataset and new thermodynamic models for amphibole, white mica, and clinopyroxene, with the software THERMOCALC. Minerals considered for the grids include garnet, omphacite, diopside, jadeite, hornblende, actinolite, glaucophane, zoisite, lawsonite, kyanite, coesite, quartz, talc, muscovite, paragonite, biotite, chlorite, and plagioclase. Compatibility diagrams are used to illustrate the phase relationships in the grids. Coesite-bearing eclogites and a whiteschist from China are used to demonstrate the ability of pseudosections to model phase relationships in natural ultrahigh-pressure metamorphic rocks. Under water-saturated conditions, chlorite-bearing assemblages in Mg- and Al-rich eclogites are stable at lower temperatures than in Fe-rich eclogites. The relative temperature stability of the three amphiboles is hornblende > actinolite > glaucophane (amphibole names used sensu lato*). Talc-bearing assemblages are stable only at low temperature and high pressure in Mg- and Al-rich eclogites. For most eclogite compositions, talc coexists with lawsonite, but not zoisite, in the stability field of coesite. Water content contouring of pressure–temperature pseudosections, along with appropriate geotherms, provides new constraints concerning dehydration of such rocks in subducting slabs. Chlorite and lawsonite are two important H_2O-carriers in subducting slabs. Depending on bulk composition and pressure–temperature path, amphibole may or may not be a major H_2O-carrier to depth. In most cases, dehydration to make ultrahigh-pressure eclogites takes place gradually, with H_2O content controlled by divariant or higher variance assemblages. Therefore, fluid fluxes in subduction zones are likely to be continuous, with the rate of dehydration changing with changing pressure and temperature. Further, eclogites of different bulk compositions dehydrate differently. Dehydration of Fe-rich eclogite is nearly complete at relatively shallow depth, whereas Mg- and Al-rich eclogites dehydrate continuously down to greater depth.*

KEY WORDS: *dehydration; eclogites; phase relations; THERMOCALC; UHP metamorphism; whiteschists*

INTRODUCTION

The past two decades have witnessed widespread discoveries and an increasingly extensive study of ultrahigh-pressure (UHP) metamorphic rocks, including coesite and/or diamond-bearing eclogites, whiteschists, felsic gneisses, and garnet-bearing ultramafic rocks, that are distributed along many orogenic belts worldwide (Chopin, 2003). Considerable efforts have been made to establish the pressure (P)–temperature (T) conditions experienced by such rocks. However, identification of UHP metamorphic rocks has been largely limited to searching for a few mineral indicators, e.g. the presence of coesite and/or diamond [see Chopin & Sobolev (1995) for review], because most other minerals are stable over wide P–T ranges (e.g. Massonne, 1995), with

*Corresponding author. E-mail: jjyang@mail.igcas.ac.cn

their stability dependent on the mineral assemblage they occur in, as well as bulk composition. Some mineral assemblages can also be used for identification of UHP conditions via geothermobarometry. These include mu + ta + ky + coe, g + mu + coe and g + o + ky + coe (Massonne & Schreyer, 1989; Harley & Carswell, 1995; Poli & Schmidt, 1998; Ravna & Terry, 2004; see the caption of Fig. 1 for mineral abbreviations, with, in addition, ru for rutile). However, such mineral assemblages are not always present, and obviously the necessity for coesite to be in the assemblage means that the UHP character of the rock is already established. In contrast, the phase diagram approach allows a systematic understanding of the stability of mineral assemblages and, when combined with detailed petrography, is a more useful and general way of delineating the *P–T* conditions experienced by rocks. Moreover, analysis of phase relationships is the basis for thermobarometry (i.e. minerals involved in a thermometer or a barometer must be known to belong to the same assemblage).

Phase transformations in subducting slabs, including dehydration, decarbonation, and partial melting, are key issues for understanding fluid flux, the cause of earthquakes in subduction zones, metasomatism in the mantle wedge and arc magmatism. Although some experimental work has been carried out on crustal compositions at UHP conditions (e.g. Poli & Schmidt, 1998; Schmidt & Poli, 1998; Schmidt *et al.*, 2004), uncertainties remain in the phase relations. Thermodynamic calculations provide an additional or alternative approach. For example, Delany & Helgeson (1978) carried out phase equilibria calculations involving end-member minerals up to 100 kbar. Guiraud *et al.* (1990) calculated a *P–T* grid for the CaO-free system Na_2O–FeO–MgO–Al_2O_3–SiO_2–H_2O (NFMASH) up to 50 kbar. Massonne (1995) presented a *P–T* projection for the simple end-member MASH system in the *P–T* range 10–70 kbar and 400–900°C. Hacker *et al.* (2003*a*) calculated phase diagrams for eclogites in the system Na_2O–CaO–K_2O–FeO–Fe_2O_3–MgO–Al_2O_3–SiO_2–H_2O (NCKFMASHO) up to 80 kbar.

With the growth of thermodynamic databases (e.g. Holland & Powell, 1998) and the development of improved mixing models for minerals and fluids (Powell *et al.*, 1998; Coggon & Holland, 2002; Holland & Powell, 2003; Dale *et al.*, 2005), it is now possible to calculate phase diagrams for more geologically appropriate systems involving complex solid solutions (Powell *et al.*, 1998). Phase relations in NCFMASH relevant to eclogites and blueschists in the *P–T* range 8–23 kbar and 400–600°C were calculated by Carson *et al.* (1999) and Wei *et al.* (2003), and were applied to natural eclogites from various localities. Rebay & Powell (2002) calculated a general *P–T* grid in this system for pressures up to 28 kbar and 640°C. These studies were, however, restricted to the K-free system and used activity–composition models for the minerals that have been superceded. The aim of this study is to calculate petrogenetic grids and compatibility diagrams using new activity–composition models for amphibole (Dale *et al.*, 2005), white mica (Coggon & Holland, 2002) and clinopyroxene (Holland & Powell, 1996) to provide a general framework for the phase relations relevant to eclogites and whiteschists in the system Na_2O–CaO–K_2O–FeO–MgO–Al_2O_3–SiO_2–H_2O (NCKFMASH) in the *P–T* range 15–45 kbar and 550–900°C, which is appropriate for rocks cropping out in HP and UHP metamorphic belts. In addition to the phases considered in earlier studies, the new grid involves diopside, jadeite, talc, biotite, muscovite, and zoisite. The importance of muscovite is obvious because of the common occurrence of phengite in UHP rocks of crustal composition. Zoisite is used instead of clinozoisite given the high *P–T* range considered here. Application of such *P–T* grids to natural eclogites and whiteschists is best made in the form of pseudosections. All the calculations were undertaken using the software THERMOCALC 3.25 (Powell *et al.*, 1998) along with the most recent dataset (Holland & Powell, 1998, upgrade 5.5, November 2003). The thermodynamics of the end-members involved are appropriate to at least 100 kbar (Holland & Powell, 1998). With the exception of white mica, the *a–x* relationships of the minerals are taken to be *P*-independent, and the interaction energies *T*-independent, as presented in Electronic Appendix 1 (available for downloading from http://www.petrology.oupjournals.org), along with the THERMOCALC datafile that represents these relationships.

GENERAL PHASE RELATIONS

In the system NCKFMASH for the *P–T* range and rock-types of interest, garnet, omphacite, diopside, jadeite, hornblende, actinolite, glaucophane, zoisite, lawsonite, kyanite, coesite, quartz, talc, muscovite, paragonite, biotite, chlorite and plagioclase are considered. Here we follow, for example, Dale *et al.* (2005) and Štípská & Powell (2005), and use *sensu lato* mineral names in considering calculated phase equilibria, and, therefore, also the minerals in rocks, so muscovite is used regardless of celadonite content, and amphibole naming is solvus-based (see Dale *et al.*, 2005). Thus, for example, actinolite extends to winchitic composition, and hornblende to barroisitic composition. The distinction between diopside, omphacite and jadeite is also solvus-based, with the boundaries given by the solvus tops (Štípská & Powell, 2005). For both amphibole and clinopyroxene, the sub-solvus top naming is continued to temperatures above the solvus tops, even though there the compositional distinctions between the minerals no longer exist.

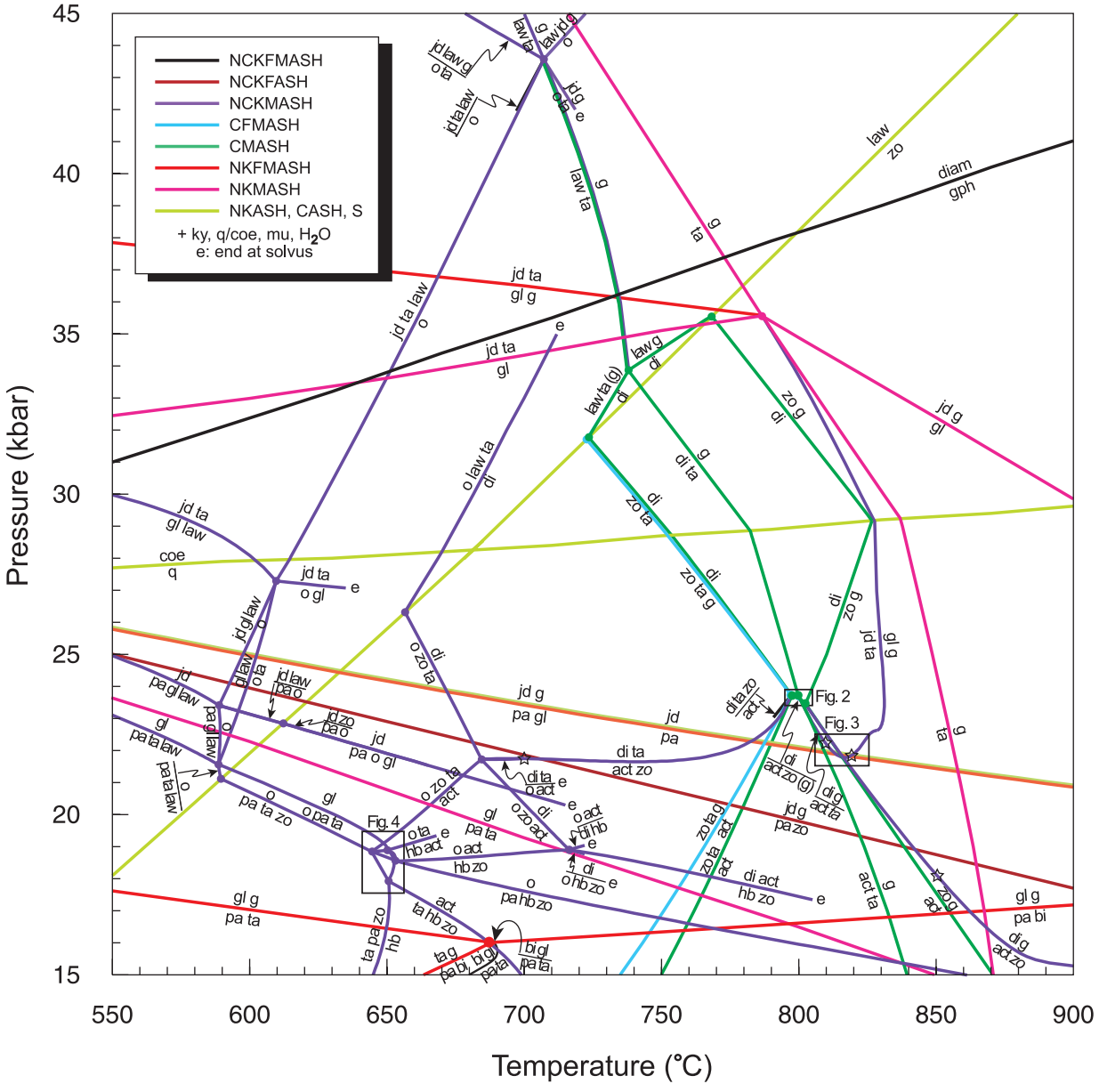

Fig. 1. *P–T* projection with, in excess, kyanite, muscovite (where Na_2O and K_2O are involved), quartz/coesite, and H_2O in the subsystems CMASH, CFMASH, NKASH, NKMASH, NKFMASH, and NCKMASH. The small letter 'e' marks where a univariant reaction terminates when amphibole or clinopyroxene exits their respective solvi. Stars indicate the position of a singular point; the phase in italics changes side of the univariant line when a singular point is crossed. Short black lines emanating from subsystem invariant points connect with the full-system univariant reactions in Fig. 5. The diam = gph transition is shown by a black line. Mineral abbreviations: g, garnet; o, omphacite; jd, jadeite; di, diopside; act, actinolite; hb, hornblende; gl, glaucophane; mu, muscovite; pa, paragonite; bi, biotite; ta, talc; chl, chlorite; pl, plagioclase; law, lawsonite; ky, kyanite; zo, zoisite; coe, coesite; q, quartz; diam, diamond; gph, graphite.

Whereas *P–T* and other pseudosections are the way to show the phase relations for a given rock composition in a model system (Powell *et al.*, 2005), a *P–T* projection ('*P–T* grid') shows the phase relations for all the compositions in the system. Usually the system is constrained by specifying that certain phases are always present ('in excess'). Constraining larger systems with many phases, such as NCKFMASH, is the way to make their *P–T* grids manageable and useable (Wei & Powell, 2006). *P–T* grids, involving only univariant lines and invariant points, can often be better visualized with compatibility diagrams (compositional sections at constant *P–T*). Such diagrams need to involve systems sufficiently constrained so that the resulting system is effectively ternary. It can then be portrayed in two dimensions. In this context, compatibility diagrams show

the phase relations for all bulk compositions in the constrained system at the specified P–T.

Generally a detailed determination of subsystem equilibria is not necessary for understanding a full system: subsystem equilibria are not seen by full-system bulk compositions in pseudosections, unless they are also degenerate in the full system (e.g. law = zo + ky + q + H_2O in NCKFMASH involves fewer than nine phases in the eight-component system). However, subsystem equilibria determine the phase relations along the edges of compatibility diagrams, and, as tie triangles emanate from subsystem univariant reactions, they are also reflected in the interior behaviour of compatibility diagrams. Given that the commonly occurring UHP assemblages are high variance, and indeed that there are no full-system univariants in the high P–T range (see below), the subsystem equilibria provide a framework for understanding the full-system high-variance mineral equilibria.

For the full-system P–T grid, garnet, kyanite, muscovite, coesite/quartz, and H_2O are taken to be in excess. The requirement regarding garnet is relaxed in considering the subsystems of NCKFMASH. Taking kyanite to be in excess means that the grids are directly applicable only to relatively Al-rich bulk compositions, noting that kyanite occurs in a wider range of bulk compositions to UHP conditions. Given that the main concern here is eclogites of basaltic composition, carpholite and chloritoid, typical of metapelites, are not included in the grids. Chlorite and plagioclase, which are relevant, but only at lower temperature and lower pressure respectively, are also not included in the grids, to simplify the phase relations given that their stability is far from the primary P–T range of interest. However, for the calculation of pseudosections, for example for the UHP rocks considered below, no constraint needs to be made on the system.

At higher temperatures, the calculated equilibria will be metastable with respect to melt. In the absence of a thermodynamic model for melt in metabasic systems, melt-bearing equilibria cannot be calculated. In addition, in the absence of an activity–composition model for solute-rich hydrous fluids at high pressure, the fluid in the calculations is treated as pure H_2O.

A P–T projection in the range 15–45 kbar and 550–900°C is presented for the subsystems leading up to the full NCKFMASH system. The focus is first on the NCKMASH system and its constituent subsystems, including compatibility diagrams for NCKMASH. Then the FeO-bearing subsystems are considered. A P–T projection is then presented for the full NCKFMASH system, along with compatibility diagrams for this system. It is important to register how invariant points in smaller subsystems become the starting point for univariant lines in systems with one more component (oxide). Moreover, if there are two (or more) such larger systems then there will be two (or more) different univariant lines emanating from them. The in-excess phases are not included in assemblages and reactions when they are written below. Pressure, temperature, and composition parameters of the minerals at the invariant points in the different systems are given in Table 1. Compatibility diagrams are used to illustrate the dependence of phase relations on bulk composition with changing P–T for selected areas in the various subsystem P–T projections in Electronic Appendix 2, available for downloading from http://www.petrology.oupjournals.org.

NCKMASH

In this system (and also in the full system) there are several reactions that are effectively unary. In S there is coe = q, in CASH there is law = zo, and in NKASH there is jd = pa. These reactions divide up the P–T plane and they are all important boundaries defining the stabilities of coesite, quartz, lawsonite, zoisite, jadeite, and paragonite.

CMASH

Six stable invariant points exist in this subsystem involving lawsonite, actinolite, garnet, talc, zoisite and diopside with the in-excess phases (Fig. 1, Table 1). Three invariant points at lower pressure cluster closely, and are shown in more detail in Fig. 2. In this system, actinolite and talc are solid solutions involving Tschermak's substitutions ($AlAlMg_{-1}Si_{-1}$), and garnet is a solid solution involving $CaMg_{-1}$. The univariant reactions law + ta = g, di + ta = g, and act + ta = g define the lower temperature limit of Ca–Mg garnet. The stability of pure diopside is defined by a polygonal region in the range 23–35 kbar and 720–830°C; that of actinolite is confined to a polygonal region below 23 kbar and between 750 and 870°C (Fig. 1).

NKMASH

This subsystem involves jadeite, garnet, glaucophane, talc and paragonite with the in-excess phases. Talc, paragonite, and muscovite are solid solutions, but all other phases are pure end-members. There is one stable invariant point in this subsystem in the P–T range of interest (Fig. 1). Two univariant reactions emanating from this point define the lower temperature limit of pyrope and the upper temperature limit of talc, whereas the other two univariant reactions define the upper pressure limit of glaucophane. The lower pressure limit of glaucophane is defined by pa + ta = gl.

Table 1: Calculated results for stable invariant equilibria in the various subsystems and in the full system

Inv. pt.	Phases	*P* (kbar)	*T* (°C)	x(g)	z(g)	x(di)	J(di)	N(di)	x(o)	J(o)	N(o)	x(jd)	J(jd)	N(jd)	x(act)	y(act)	z(act)	a(act)	x(hb)	y(hb)	z(hb)	a(hb)
CMASH																						
(+ ky, coe/q, fluid)																						
1	g, di, zo, law	35·56	768·3		0·305																	
2	g, ta, di, law	33·86	738·0		0·22																	
3	ta, di, zo, law	31·78	723·5																			
4	act, g, ta, di	23·73	799·8		0·176											0·053						
5	act, ta, di, zo	23·72	797·5													0·053						
6	act, g, di, zo	23·46	802·5		0·177											0·055						
CFMASH																						
(+ ky, coe/q, fluid)																						
7	g, di, ta, zo, law	31·72	722·7	0·105	0·260	0·009																
8	act, g, di, ta, zo	23·73	797·3	0·008	0·179	0·001									0·001	0·053						
NKMASH																						
(+ ky, mu, coe, fluid)																						
9	ta, jd, py, gl	34·78	792·9																			
NKFMASH																						
(+ ky, mu, q, fluid)																						
10	bi, pa, ta, gl, g	16·02	688·8	0·518																		
NCKMASH																						
(+ ky, mu, coe/q, fluid)																						
11	o, jd, g, ta, law	43·60	706·9		0·061					0·656	0·209		0·656	0·208								
12	o, jd, ta, gl, law	27·29	609·6							0·582	0·345		0·815	0·043								
13	o, di, ta, zo, law	26·33	656·6				0·222	0·064		0·399	0·304											
14	pa, o, jd, gl, law	23·42	588·8							0·575	0·360		0·830	0·037								
15	pa, o, jd, zo, law	22·86	612·1							0·583	0·343		0·813	0·044								
16	o, di, ta, act, zo	21·73	684·5				0·249	0·084		0·382	0·271					0·190	0·213	0·058				
17	o, di, hb, act, zo	18·91	716·4				0·294	0·130		0·349	0·210					0·250	0·240	0·097		0·634	0·286	0·445
18	pa, o, ta, gl, law	21·57	588·6							0·515	0·397											
19	pa, o, ta, zo, law	21·12	589·5							0·506	0·398											
20	pa, o, ta, gl, act	18·89	650·0							0·485	0·367					0·400	0·413	0·103				
21	pa, o, ta, act, zo	18·85	644·4							0·481	0·369					0·330	0·350	0·087				
22	pa, o, hb, act, zo	18·57	653·0							0·478	0·364					0·336	0·349	0·094		0·718	0·471	0·374
23	pa, ta, hb, act, zo	17·93	650·5													0·290	0·302	0·084		0·723	0·411	0·429

Table 1: Continued

Inv. pt.	Phases	*P* (kbar)	*T* (°C)	x(g)	z(g)	x(di)	J(di)	N(di)	x(o)	J(o)	N(o)	x(jd)	J(jd)	N(jd)	x(act)	y(act)	z(act)	a(act)	x(hb)	y(hb)	z(hb)	a(hb)
NCKFMASH																						
(+ g, ky, mu, coe/q, fluid)																						
23	o, jd, ta, gl, law	31·41	632·6	0·483	0·115				0·090	0·594	0·323	0·103	0·794	0·055								
24	o, di, ta, zo, law	26·01	652·6	0·474	0·276	0·062	0·221	0·064	0·070	0·398	0·305											
25	pa, o, jd, gl, law	23·04	600·6	0·803	0·263				0·264	0·587	0·344	0·289	0·813	0·047								
26	o, di, ta, act, zo	23·02	670·5	0·452	0·246	0·067	0·238	0·076	0·075	0·388	0·285				0·065	0·196	0·223	0·063				
27	pa, o, jd, zo, law	22·77	611·0	0·835	0·321				0·303	0·592	0·334	0·327	0·805	0·051								
28	o, ta, gl, zo, law	22·60	608·7	0·620	0·264				0·118	0·482	0·387											
29	pa, o, gl, zo, law	21·84	598·9	0·769	0·291				0·214	0·534	0·385											
30	o, ta, gl, act, zo	21·45	632·1	0·573	0·249				0·110	0·469	0·371				0·105	0·325	0·359	0·089				
31	o, di, hb, act, zo	19·87	708·1	0·432	0·227	0·078	0·284	0·121	0·082	0·355	0·223				0·081	0·277	0·266	0·115	0·112	0·603	0·316	0·406
32	pa, o, hb, gl, zo	19·19	655·2	0·646	0·256				0·163	0·500	0·366								0·251	0·844	0·673	0·392
33	pa, ta, gl, zo, law	18·67	557·4	0·749	0·243																	
34	pa, ta, hb, gl, zo	17·48	601·4	0·673	0·230														0·236	0·773	0·518	0·409

Inv.pt.	Phases	*P* (kbar)	*T* (°C)	x(gl)	y(gl)	z(gl)	a(gl)	x(ta)	y(ta)	x(mu)	y(mu)	na(mu)	x(pa)	y(pa)	na(pa)	x(bi)	y(bi)	N(bi)
CMASH																		
(+ ky, coe/q, fluid)																		
1	g, di, zo, law	35·56	768·3															
2	g, ta, di, law	33·86	738·0						0·037									
3	ta, di, zo, law	31·78	723·5						0·038									
4	act, g, ta, di	23·73	799·8						0·066									
5	act, ta, di, zo	23·72	797·5						0·066									
6	act, g, di, zo	23·46	802·5															
CFMASH																		
(+ ky, coe/q, fluid)																		
7	g, di, ta, zo, law	31·72	722·7					0·005	0·038									
8	act, g, di, ta, zo	23·73	797·3					0·001	0·066									
NKMASH																		
(+ ky, mu, coe, fluid)																		
9	ta, jd, py, gl	34·78	792·9						0·041		0·473	0·028						

JOURNAL OF PETROLOGY VOLUME 47 NUMBER 10 OCTOBER 2006

Inv.pt.	Phases	*P* (kbar)	*T* (°C)	x(gl)	y(gl)	z(gl)	a(gl)	x(ta)	y(ta)	x(mu)	y(mu)	na(mu)	x(pa)	y(pa)	na(pa)	x(bi)	y(bi)	N(bi)
NKFMASH																		
(+ ky, mu, q, fluid)																		
10	bi, pa, ta, gl, g	16·02	688·8	0·280	0·925	0·9997	0·174	0·071	0·074	0·190	0·839	0·196	0·190	0·995	0·946	0·207	0·151	0·336
NCKMASH																		
(+ ky, mu, coe/q, fluid)																		
11	o, jd, g, ta, law	43·60	706·9						0·022		0·323	0·006						
12	o, jd, ta, gl, law	27·29	609·6		0·894	0·947	0·107		0·032		0·595	0·040						
13	o, di, ta, zo, law	26·33	656·6						0·039		0·607	0·022						
14	pa, o, jd, gl, law	23·42	588·8		0·904	0·954	0·103				0·731	0·095		0·994	0·981			
15	pa, o, jd, zo, law	22·86	612·1								0·808	0·119		0·996	0·975			
16	o, di, ta, act, zo	21·73	684·5						0·054		0·708	0·051						
17	o, di, hb, act, zo	18·91	716·4								0·776	0·091						
18	pa, o, ta, gl, law	21·57	588·6		0·869	0·914	0·095		0·041		0·754	0·104		0·995	0·978			
19	pa, o, ta, zo, law	21·12	589·5						0·042		0·764	0·107		0·996	0·977			
20	pa, o, ta, gl, act	18·89	650·0		0·644	0·603	0·172		0·058		0·807	0·151		0·995	0·963			
21	pa, o, ta, act, zo	18·85	644·4						0·057		0·808	0·148		0·995	0·964			
22	pa, o, hb, act, zo	18·57	653·0								0·815	0·156		0·995	0·961			
23	pa, ta, hb, act, zo	17·93	650·5						0·061		0·825	0·161		0·996	0·959			
NCKFMASH																		
(+ g, ky, mu, coe/q, fluid)																		
23	o, jd, ta, gl, law	31·41	632·6	0·144	0·886	0·952	0·134	0·034	0·028	0·114	0·489	0·021						
24	o, di, ta, zo, law	26·01	652·6					0·031	0·040	0·099	0·600	0·022						
25	pa, o, jd, gl, law	23·04	600·6	0·412	0·904	0·975	0·154			0·284	0·766	0·106	0·284	0·995	0·978			
26	o, di, ta, act, zo	23·02	670·5					0·034	0·049	0·104	0·667	0·039						
27	pa, o, jd, zo, law	22·77	611·0							0·322	0·798	0·117	0·322	0·995	0·976			
28	o, ta, gl, zo, law	22·60	608·7	0·189	0·823	0·876	0·114	0·049	0·041	0·146	0·687	0·056						
29	pa, o, gl, zo, law	21·84	598·9	0·347	0·894	0·959	0·143			0·239	0·774	0·110	0·239	0·995	0·976			
30	o, ta, gl, act, zo	21·45	632·1	0·164	0·754	0·797	0·122	0·047	0·048	0·138	0·713	0·067						
31	o, di, hb, act, zo	19·87	708·1							0·114	0·745	0·072						
32	pa, o, hb, gl, zo	19·19	655·2	0·256	0·848	0·834	0·226			0·192	0·813	0·153	0·192	0·995	0·963			
33	pa, ta, gl, zo, law	18·67	557·4	0·309	0·877	0·929	0·115	0·074	0·044	0·204	0·797	0·109	0·204	0·998	0·974			
34	pa, ta, hb, gl, zo	17·48	601·4	0·252	0·820	0·842	0·147	0·067	0·054	0·184	0·819	0·138	0·184	0·997	0·965			

NCKMASH

Phases in this subsystem include lawsonite, zoisite, garnet, diopside, omphacite, jadeite, actinolite, hornblende, glaucophane, talc and paragonite with the in-excess phases. There are 13 stable invariant points in the NCKMASH subsystem (Fig. 1, Table 1). A univariant reaction jd + ta = gl + g emanates from the NKMASH subsystem invariant point. This reaction runs first to lower pressure but then runs to higher pressure to connect to the CMASH subsystem invariant point involving diopside, talc, actinolite, and garnet (Fig. 1). Along this univariant line the compositions of amphibole and pyroxene change continuously from glaucophane and jadeite (at the NKMASH invariant point) to actinolite and diopside (at the CMASH invariant point). Figure 3 shows the phase relations in the immediate *P–T* region around the lower pressure part of this reaction, with corresponding compatibility diagrams for each of the fields given in Electronic Appendix 2. Contributing to the complexity of this region is the way in which the amphibole one-phase field is dissected by the two singular reactions emanating from the two singular points (marked by stars in Fig. 3).

Several other univariant reactions involving garnet emanate from the CMASH invariant points. The univariant reaction involving lawsonite, talc, and garnet is degenerate in NCKMASH, and corresponds to the same univariant reaction in the CMASH subsystem. It terminates at an invariant point at about 43·5 kbar and 705°C (Fig. 1). A new degenerate univariant reaction emanating from this point involves the same phases and defines the lower temperature stability of Ca–Mg garnet at higher pressure. Apart from this invariant point, all the other 12 invariant points are at temperatures lower than the stability field of garnet, and thus are garnet-free. The degenerate reaction law = zo defines the stability limit of lawsonite and zoisite, with kyanite, muscovite, quartz/coesite, and H_2O in excess (Fig. 1). The stability of diopside extends to much lower temperature in this subsystem compared with that in CMASH and CFMASH. The stability of omphacite is located at even lower temperature, and that of jadeite still lower (Fig. 1). Likewise, the lower temperature and/or pressure limits of actinolite, hornblende, and glaucophane are delineated by univariant reactions at lower pressures. Four invariant points at low pressures cluster closely around 650°C, and are shown in Fig. 4, with corresponding compatibility diagrams in Electronic Appendix 2, to clarify the relationships there. In contrast to Fig. 3, the temperature range in Fig. 4 is below the top of the amphibole solvus (shown by an 'e' in Figs 1, 5 and 6), noting that there are univariant reactions involving two amphiboles. In this region, the lower temperature stability limits of actinolite and hornblende intersect. Again, contributing to the complexity is the singular reaction connecting the two singular points (marked by stars in Fig. 4) that divides the hornblende one-phase field, with the resulting two hornblendes reacting out down temperature by two different reactions (see Electronic Appendix 2 for compatibility diagrams). Up pressure along the o + pa + ta = hb reaction line, the hornblende composition changes continuously into that of glaucophane (Figs 1 and 4).

Univariant reactions also define the stability fields of some mineral assemblages in this subsystem. For example, the stability fields of the assemblage ta + di/o/jd is constrained. The assemblage ta + jd is confined to $\leq$830°C and $\geq$23 kbar, whereas the assemblage g + gl in this subsystem is limited to higher *P–T* conditions.

In this subsystem, univariant reactions involving two phases of the same structure, such as diopside, omphacite or jadeite, and actinolite, hornblende or glaucophane, terminate when the compositions of two minerals of the same structure converge and become identical, on leaving their solvus (shown by an 'e' in Fig. 1). All but one such reaction terminate at a temperature lower than 720°C. However, in the reaction di + act = zo + hb, actinolite and hornblende are distinct phases to above 800°C.

Compatibility diagrams are used to illustrate the dependence of phase relations on bulk composition with changing *P–T* for selected areas (Figs 3 and 4) in the various *P–T* projections in Electronic Appendix 2.

NCKFMASH

NCKFASH

The univariant reaction pa + zo = jd + g takes place in this subsystem (Figs 1 and 6).

CFMASH

CFMASH univariant reactions emanate from each of the CMASH invariant points, and are involved in two invariant points. One of the points is located at the law = zo reaction, with which three degenerate univariant reactions coincide (Fig. 1). The other point is located at a lower pressure (Fig. 2, Table 1). In this subsystem, diopside, actinolite, garnet, and talc involve $FeMg_{-1}$. No new phase is added. The lower temperature limits of diopside and actinolite in this subsystem are close to those in the subsystem CMASH (Fig. 1).

NKFMASH

A NKFMASH univariant reaction involving jadeite, talc, glaucophane and garnet emanates from the NKMASH invariant point. It involves the same phases as in the NCKMASH subsystem reaction emanating

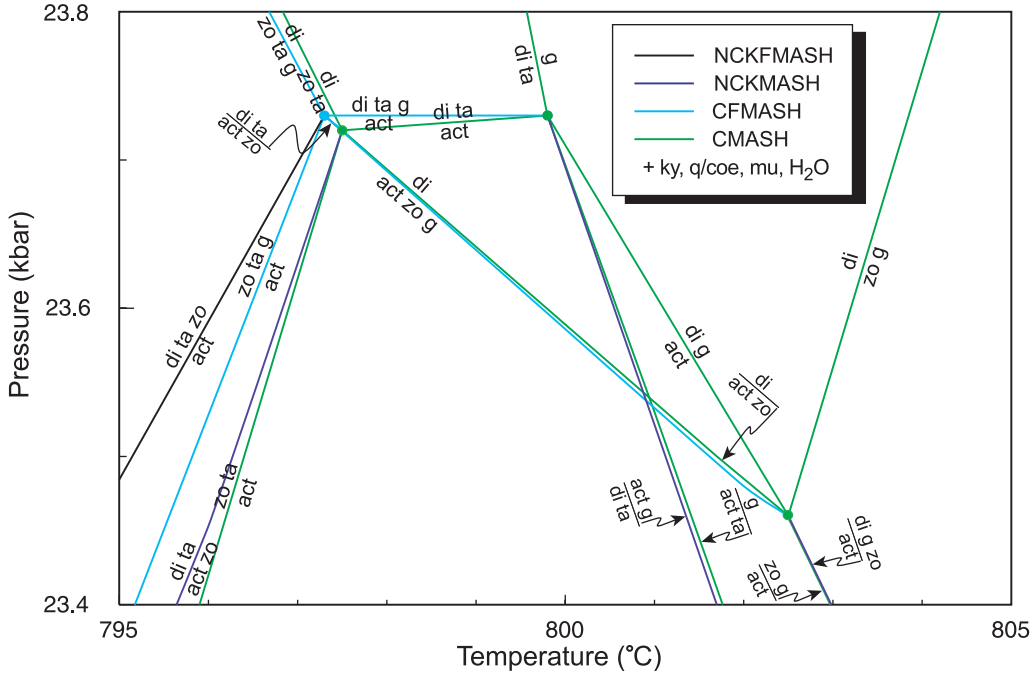

Fig. 2. Enlarged view of the *P–T* projection in Fig. 1 in the *P–T* range 23·4–23·8 kbar and 795–805°C.

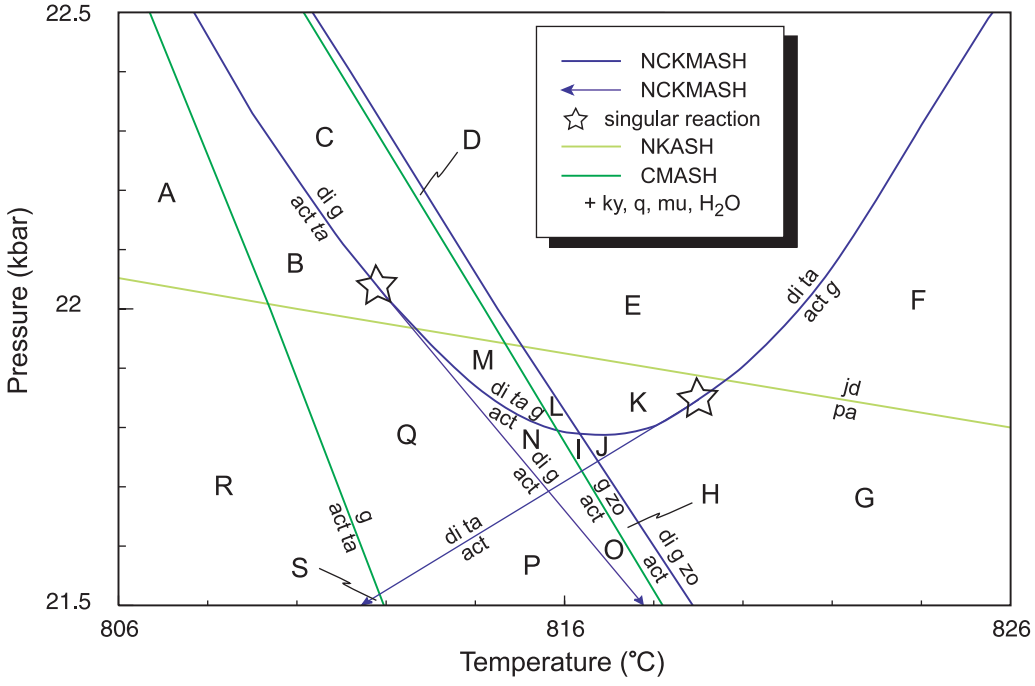

Fig. 3. Enlarged view of the *P–T* projection in Fig. 1 in the *P–T* range 21·5–22·5 kbar and 806–826°C. Capital letters A–S stand for the divariant fields they occupy.

from the same point but heads in a very different direction (see above; Fig. 1). A stable invariant point involving glaucophane, garnet, paragonite, talc, and biotite is located at low pressure. The univariant reactions in this subsystem define the upper and lower pressure stability of the assemblage gl + g. At intermediate pressures, the reaction pa + gl = jd + g almost coincides with the NKASH subsystem reaction pa = jd.

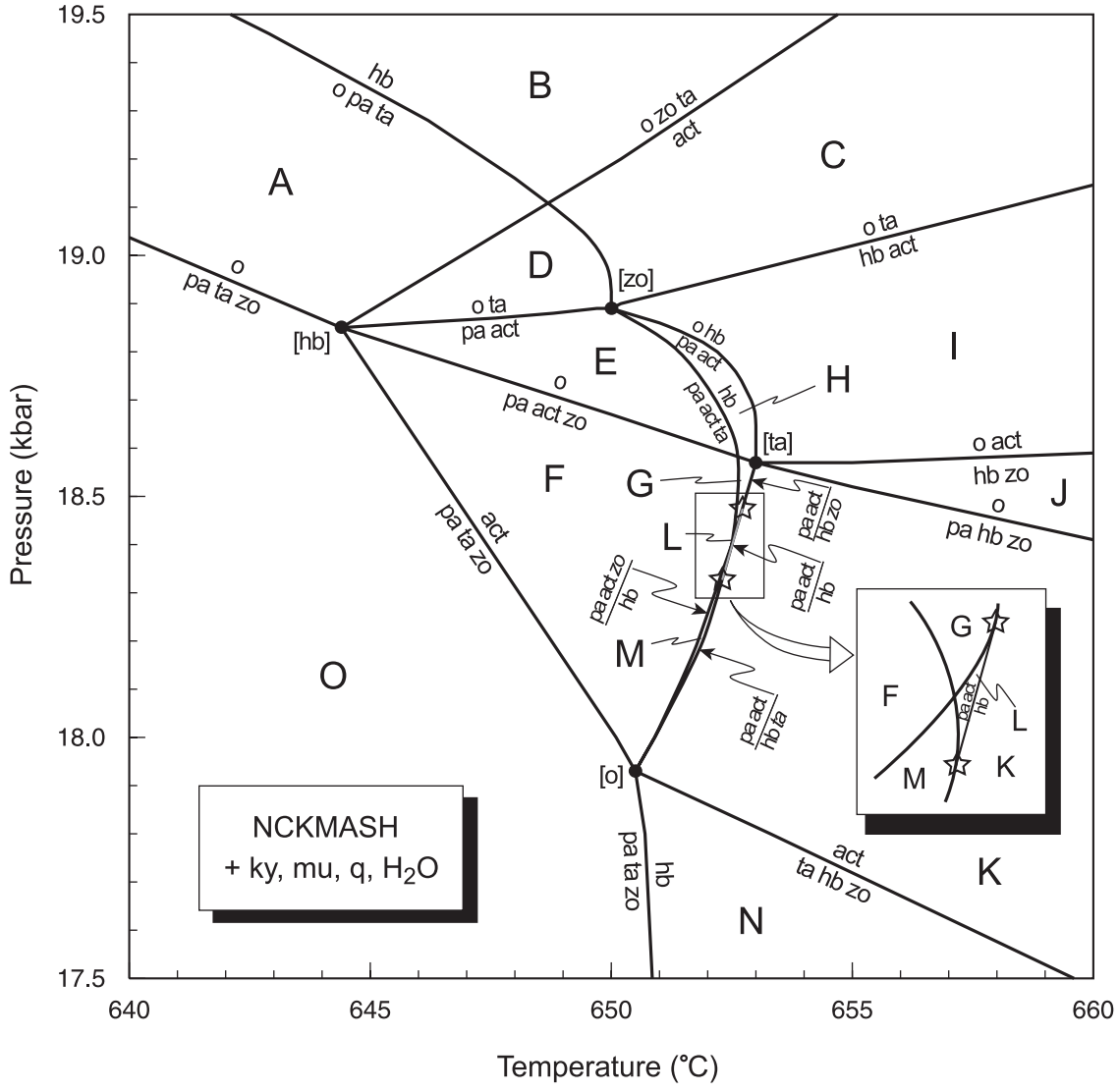

Fig. 4. Enlarged view of the *P–T* projection in Fig. 1 in the *P–T* range 17·5–19·5 kbar and 640–660°C. The composition of amphibole in the reaction o + pa + ta = hb changes from hornblende to glaucophane with increasing pressure. Capital letters A–O stand for the divariant fields they occupy.

Full system NCKFMASH

The full system is formed by adding FeO to the NCKMASH subsystem, as well as by adding MgO to NCKFASH, CaO to NKFMASH and Na_2O to (K)CFMASH. In the *P–T* projection of Fig. 5, and the compatibility diagrams of Fig. 8, garnet is treated as being in excess, in addition to kyanite, muscovite, quartz/coesite, and H_2O. Figure 6 is the enlarged part of the rectangular area in Fig. 5. A full-system univariant line emanates from each garnet-bearing invariant point in each of these subsystems. There are just three such univariant lines (Fig. 5): jd + ta + law = o, analogous to the garnet-free univariant reaction in the NCKMASH subsystem, emanates from the NCKMASH invariant point at high pressure; a univariant reaction, bi + gl = pa + ta, emanates from the NKFMASH subsystem invariant point at low pressure; and di + ta = act + zo emanates from the CFMASH subsystem invariant point at about 24 kbar and 800°C. There are 13 stable invariant points in the full system. The only invariant point at UHP conditions involves o + jd + ta + law + gl (+ g + mu + ky + coe + H_2O). Similar to the situation in the NCKMASH subsystem, full-system univariant reactions involving two phases of the same structure terminate if a reaction runs out of the respective solvus (Fig. 5), generally at temperatures lower than about 720°C.

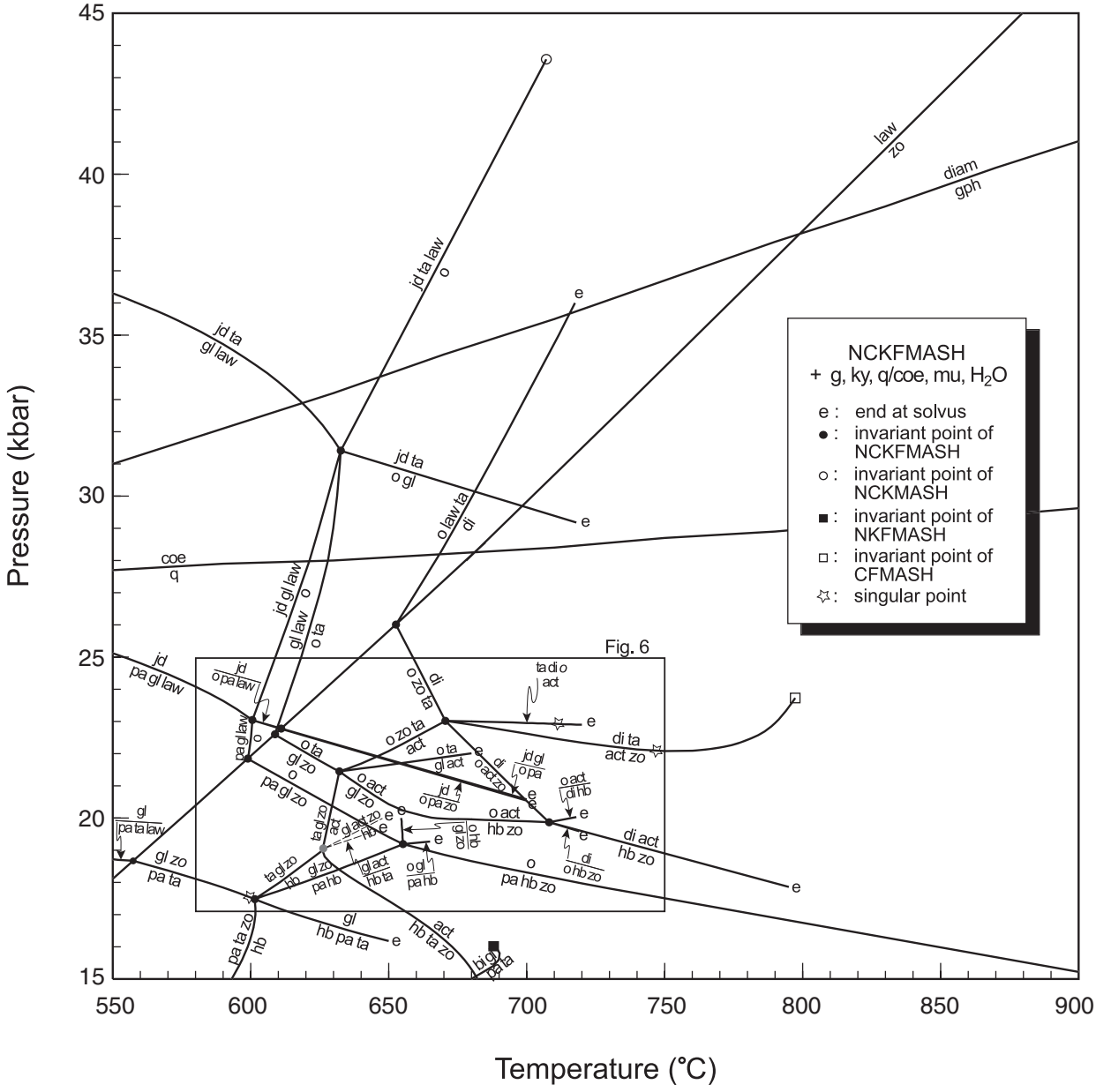

Fig. 5. *P–T* projection for the full system NCKFMASH with, in excess, garnet, kyanite, muscovite, quartz/coesite, and H_2O. The small letter 'e' marks where a univariant reaction terminates when amphibole or clinopyroxene exits their respective solvus. Filled circles denote full-system invariant points. Open circle, open square, and filled square denote, respectively, NCKMASH, CFMASH, and NKFMASH subsystem invariant points from which full-system univariant lines emanate. Star indicates the position of a singular point; the phase in italics changes side in the reaction when it crosses the singular point. Dashed lines and grey dot are deduced univariant and invariant reactions by Schreinemakers analysis. Also shown are the diam = gph and coe = q transitions.

The topology of phase relations in the full system is quite similar to that in the NCKMASH subsystem, particularly at pressures above 22 kbar (see Figs 1 and 5). The relative stability of the clinopyroxenes is similar to those in the NCKMASH subsystem, with clinopyroxene with higher jadeite component having a lower temperature stability limit. Likewise, the lower temperature and/or pressure limits of actinolite, hornblende, and glaucophane are partly delineated by the full-system reactions, and partly by subsystem reactions (Fig. 5).

As a result of the use of the new amphibole model (Dale *et al.*, 2005) and the additional involvement of jadeite, diopside, talc, biotite and zoisite (in place of clinozoisite), the phase relations of eclogite in the present study are significantly different from those in earlier work (e.g. Carson *et al.*, 1999; Wei *et al.*, 2003). The most

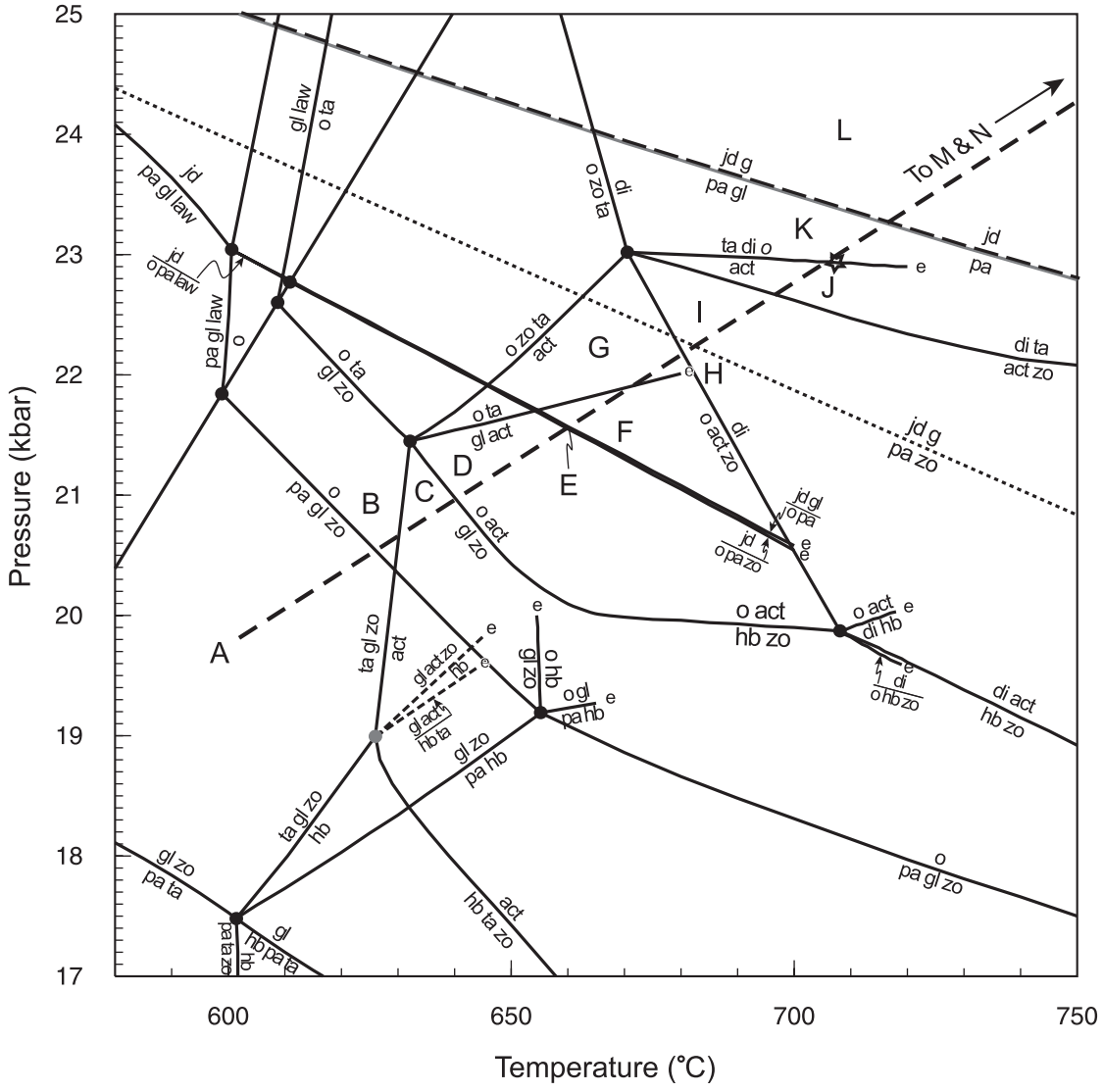

Fig. 6. Enlarged view of the *P–T* projection in Fig. 5 in the *P–T* range 17–25 kbar and 580–750°C. Dotted, grey, and dashed lines are, respectively, NCKFASH, NKFMASH, and NKASH subsystem univariant reactions (see caption of Figs 1 and 8 for details). Capital letters A–L stand for the divariant fields crossed by the thick dashed line.

notable feature of the new grid is the appearance of an invariant point at a pressure of around 19 kbar that involves all three amphiboles (Figs 5 and 6). The invariant point, however, could not be calculated and is, therefore, deduced from the calculated univariant reactions associated with it. The dashed lines related to this invariant point are also difficult to calculate and had to be deduced by Schreinemakers analysis.

Only one invariant point involving o + gl + hb + zo + pa and associated univariant reactions in the previous grids appear at 19·2 kbar and 655°C in Fig. 5; all other invariant points involve talc and/or diopside, as a result of addition of these two phases to the grid. For instance, the univariant reaction o + act = gl + zo that can be found in the previous grids terminates at an invariant point involving o + act + gl + zo + ta at 21·45 kbar and 632°C, thus cannot meet the law = zo reaction to generate the invariant point involving o + act + gl + zo/cz + law appearing in a previous grid (Carson *et al.*, 1999). The appearance of talc confines the stability of amphiboles to particular ranges (Figs 5 and 6). For instance, the high-pressure and low-temperature limits of actinolite stability are bounded by talc-bearing assemblages.

Calculated compatibility diagrams for NCKFMASH are presented using a projection plane, CFM, where C = CaO, F = 4/5 (3/4 FeO + 1/4 $KAlO_2$) + 1/5 $NaAlO_2$, and M = 3/4 MgO + 1/4 $KAlO_2$, lying

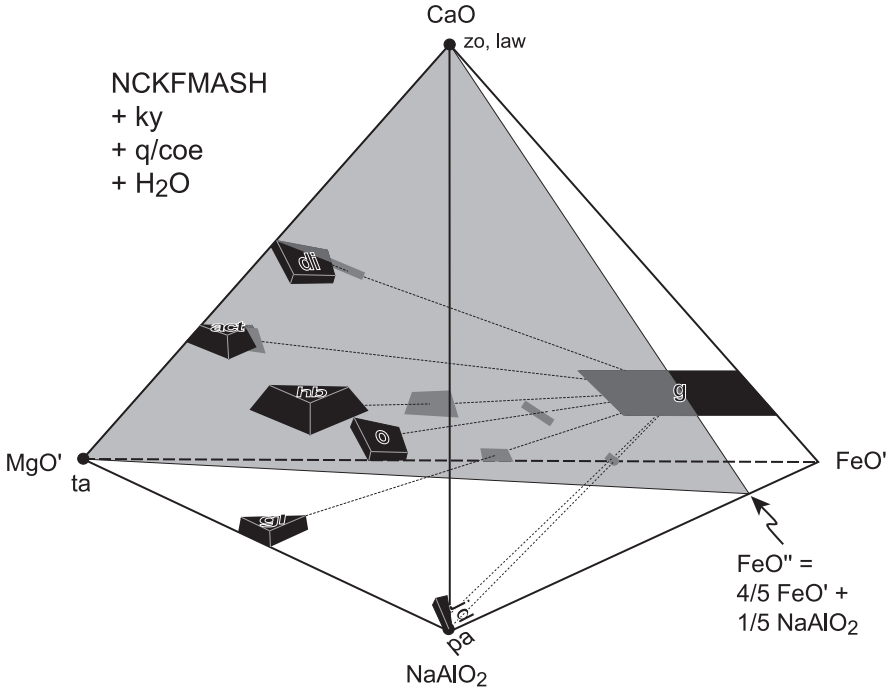

Fig. 7. Projection from garnet, kyanite, muscovite, quartz/coesite, and H_2O onto the plane CFM, where C = CaO, F = 4/5 (3/4 FeO + 1/4 $KAlO_2$) + 1/5 $NaAlO_2$, and M = 3/4 MgO + 1/4 $KAlO_2$, lying between garnet and all other phases (except biotite). Grey lozenges are compositions of the phases projected on the CFM plane.

between garnet and all other phases (Fig. 7), based on the NCKMASH projection but now projecting additionally from garnet. The NCKFMASH system can, therefore, be represented by an effective ternary CFM system, with garnet, kyanite, muscovite, quartz/coesite, and H_2O in excess. Using this projection, a series of calculated compatibility diagrams (Fig. 8) are presented for the full system along a traverse (dashed line) shown in Fig. 6. A detailed description of the full-system phase relations using these compatibility diagrams is given in Electronic Appendix 2.

APPLICATIONS

The direct application of *P–T* grids to natural rocks is limited because only some, and in some cases no reactions in a grid can take place in a particular rock, primarily because such grids display only low variance phase relationships (i.e. invariant points and univariant lines). However, the NCKFMASH grid and subsystem grids presented above serve as the fundamental framework for modelling UHP eclogites and whiteschists by means of pseudosections. Phase relationships of eclogites with compositions of Mg–Al-rich and Fe–Ti-rich gabbros and a whiteschist from the northern Qaidam Mountains (NQM) and the Su-Lu–Dabie terranes, China, are modelled using this type of phase diagram, assuming that the fluid is pure H_2O. The *P–T* histories of these UHP rocks are constrained by comparing the observed mineral assemblages with the calculated ones. Dehydration processes during subduction are then considered using the *P–T* pseudosections contoured with water content.

P–T histories of some UHP eclogites and whiteschists from China

Kyanite and coesite-bearing eclogites from Shaliuhe (NQM)

Kyanite-bearing eclogites occur in gneiss by a small river called Shaliuhe, about 40 km NE of the county town of Dulan, western China (Yang & Deng, 1994; Song *et al.*, 2003). Sample SL01 has an Mg–Al-rich gabbroic composition. The peak metamorphic assemblage consists of g + o + ky + ru + q (after coe) + mu with accessory zircon. Zoisite, kyanite, quartz, and muscovite, as well as Na-rich and Na-poor plagioclase, amphibole, chlorite and biotite, occur as inclusions in garnet. Kyanite also occurs in the matrix. Zoisite, pargasitic and barroisitic amphibole, and quartz occur as retrograde minerals. The amphiboles corrode omphacite and also cut across garnet grains. Song *et al.* (2003) reported evidence for the occurrence of coesite in the eclogite.

The *P–T* pseudosection, with muscovite and H_2O in excess, is shown in Fig. 9. This shows that under

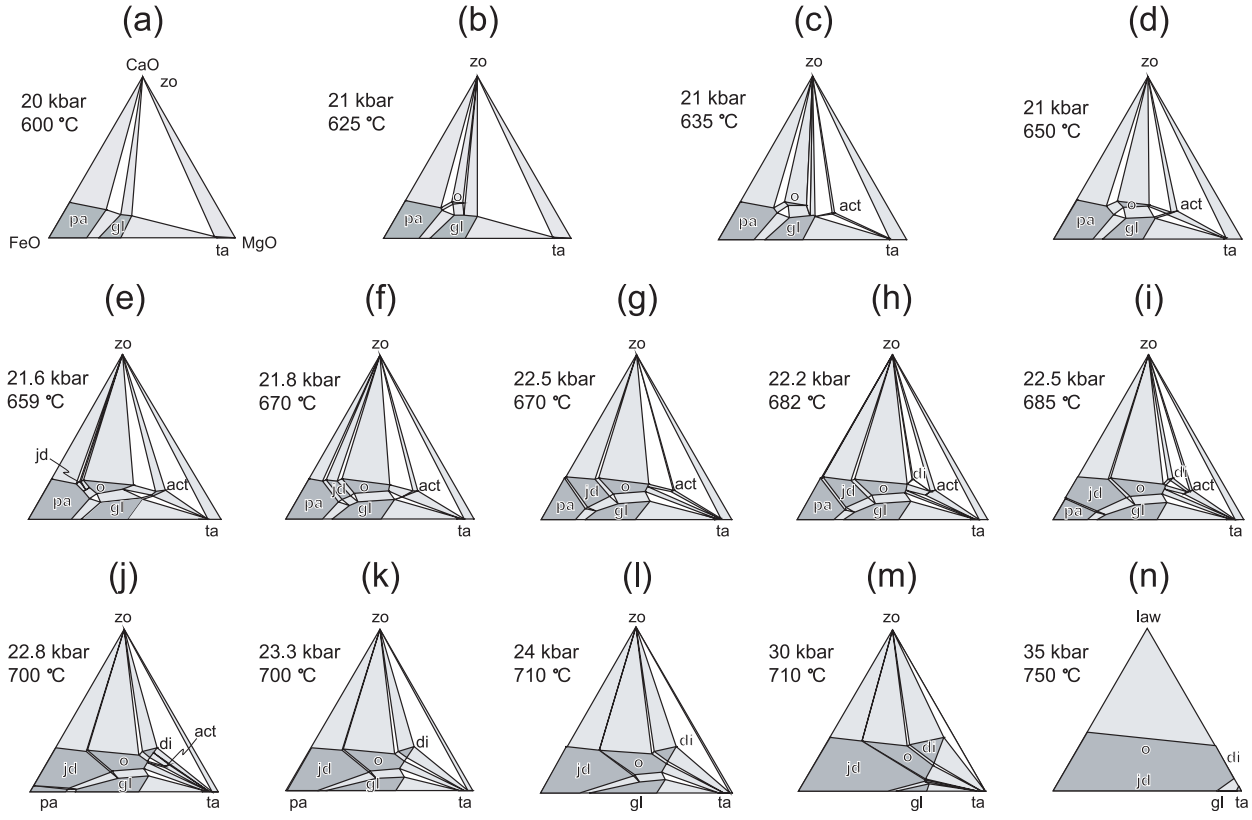

Fig. 8. Calculated compatibility diagrams for the full system NCKFMASH + g + ky + mu + q + H_2O along the dashed line in Fig. 6. The left edge of the triangle is for the subsystem NCKFASH + g + ky + mu + q + H_2O, the right edge of the triangle for the subsystem NCKMASH + g + ky + mu + q + H_2O, and the bottom edge of the triangle for the subsystem NKFMASH + g + ky + mu + q + H_2O. Divariant tie triangles are in white, trivariant fields are in light grey, and quadrivariant fields are in dark grey.

water-saturated conditions, talc-bearing assemblages are stable only at <675°C and >21 kbar. The chlorite-bearing assemblage g + o + di + chl + ta + law can be stable up to >40 kbar and <620°C. The three amphiboles, actinolite, hornblende, and glaucophane, can be in equilibrium in a narrow field at 550–560°C and 15·9–16·7 kbar. At low temperature and high pressure (>20 kbar), glaucophane-bearing assemblages react to actinolite- and lawsonite-bearing ones as pressure increases. The upper pressure stability limit of hornblende is around 20 kbar. The temperature stability of the three amphiboles is hb > act > gl. Zoisite is stable up to 28 kbar. When pressure is >37 kbar in the range 770–800°C, kyanite reacts out and the metamorphic assemblage becomes g + o + coe + H_2O.

Lawsonite is not found either as inclusions in garnet or in the matrix in the eclogites. The separate inclusions of zoisite, kyanite, and quartz in garnet do not indicate the previous existence of lawsonite (Fig. 9). This constrains the UHP part of the prograde *P–T* path to be below the stability field of lawsonite. The *P–T* conditions of peak metamorphism were either 28–37 kbar and >720°C, or *P* >37 kbar and *T* >770°C, depending on whether kyanite was present in the peak assemblage (Fig. 9). Kyanite inclusions occur only in garnet because garnet grows from 37 to 56 mol % (on a one-oxide formula basis) along the UHP part of the prograde *P–T* path, whereas the abundance of clinopyroxene decreases. The amphibole replacing omphacite and garnet, and the zoisite/clinozoisite aggregates was formed in response to fluid infiltration after the metamorphic peak. The calculated compositions of garnet, omphacite and muscovite at 35 kbar and 750°C are $Fe/(Fe + Mg)_g$ = 0·40 and $Ca/(Fe + Mg + Ca)_g$ = 0·37 ($gr_{37}py_{38}alm_{25}$), $Fe/(Fe + Mg)_o$ = 0·06 and $jd = Na/(Na + Ca)_o$ = 0·38, and $Fe/(Fe + Mg)_{mu}$ = 0·09, Si_{mu} = 3·44 and Na^A_{mu} = 0·006, respectively. The calculated $Fe/(Fe + Mg)_g$ is closer to the measured value at the rims of garnet (*c.* 0·46) than that in the cores (*c.* 0·52), although the calculated $Ca/(Fe + Mg + Ca)_g$ is much higher than the measured values at both the rims and the cores (*c.* 0·23 and *c.* 0·25, respectively). This difference may be caused by separation of abundant Ca-rich minerals (zoisite, plagioclase and amphibole) from the rock matrix by inclusion in garnet and the relatively garnet-rich cores during prograde metamorphism (Marmo *et al.*, 2002).

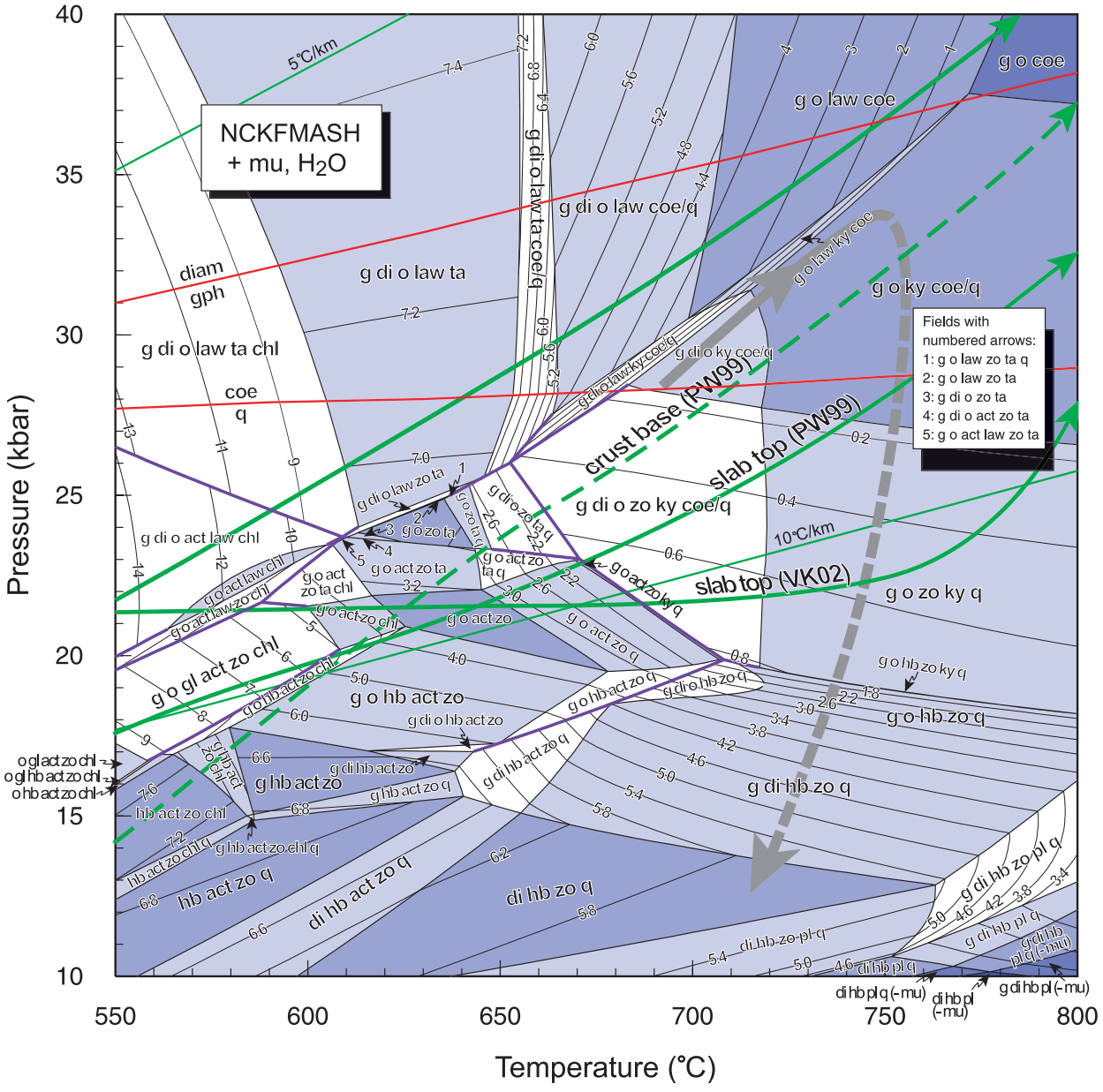

Fig. 9. *P–T* pseudosection of an Mg–Al-rich eclogite (sample SL01) from the northern Qaidam Mountains, western China, contoured for H_2O content. Bulk composition of this sample is $SiO_2 = 50{\cdot}49$, $Al_2O_3 = 10{\cdot}52$, CaO = 15·37, MgO = 15·30, FeO = 5·92, $K_2O = 0{\cdot}08$, $Na_2O = 2{\cdot}33$, in mol %. This composition is typical of Mg–Al-rich gabbros. Thick grey line is the deduced *P–T* path for this eclogite. The dashed part of the *P–T* path indicates metastable preservation of the rock from continuous re-equilibration, as a result of the absence of H_2O required for equilibrium. Univariant reactions are shown as thick dark blue lines; divariant fields are in white; trivariant, quadrivariant, quinivariant, and sextivariant fields are increasingly heavily shaded. For a discussion of the geotherms, see text (PW99, Peacock & Wang, 1999; VK02, Van Keken et al., 2002).

An average of eight omphacite analyses gives $Fe/(Fe + Mg)_o = 0{\cdot}12$ and jd = 0·34, with $Fe/(Fe + Mg)_o$ twice the calculated value but a similar jd content. A phengite analysis is $Fe/(Fe + Mg)_{mu} = 0{\cdot}07$, $Si_{mu} = 3{\cdot}44$ and $Na^A_{mu} = 0{\cdot}005$ (Song *et al.*, 2003), in good agreement with the calculated composition.

Coesite-bearing eclogite from Lanshantou (Su-Lu terrane)

This sample (RL207) is an Fe–Ti-rich eclogite. However, it contains negligible Fe^{3+} (Yang *et al.*, 1998). Garnet and omphacite are the two major minerals (about 98 vol. %). Polycrystalline quartz inclusions with or without K-feldspar are found in omphacite. Minor amphibole

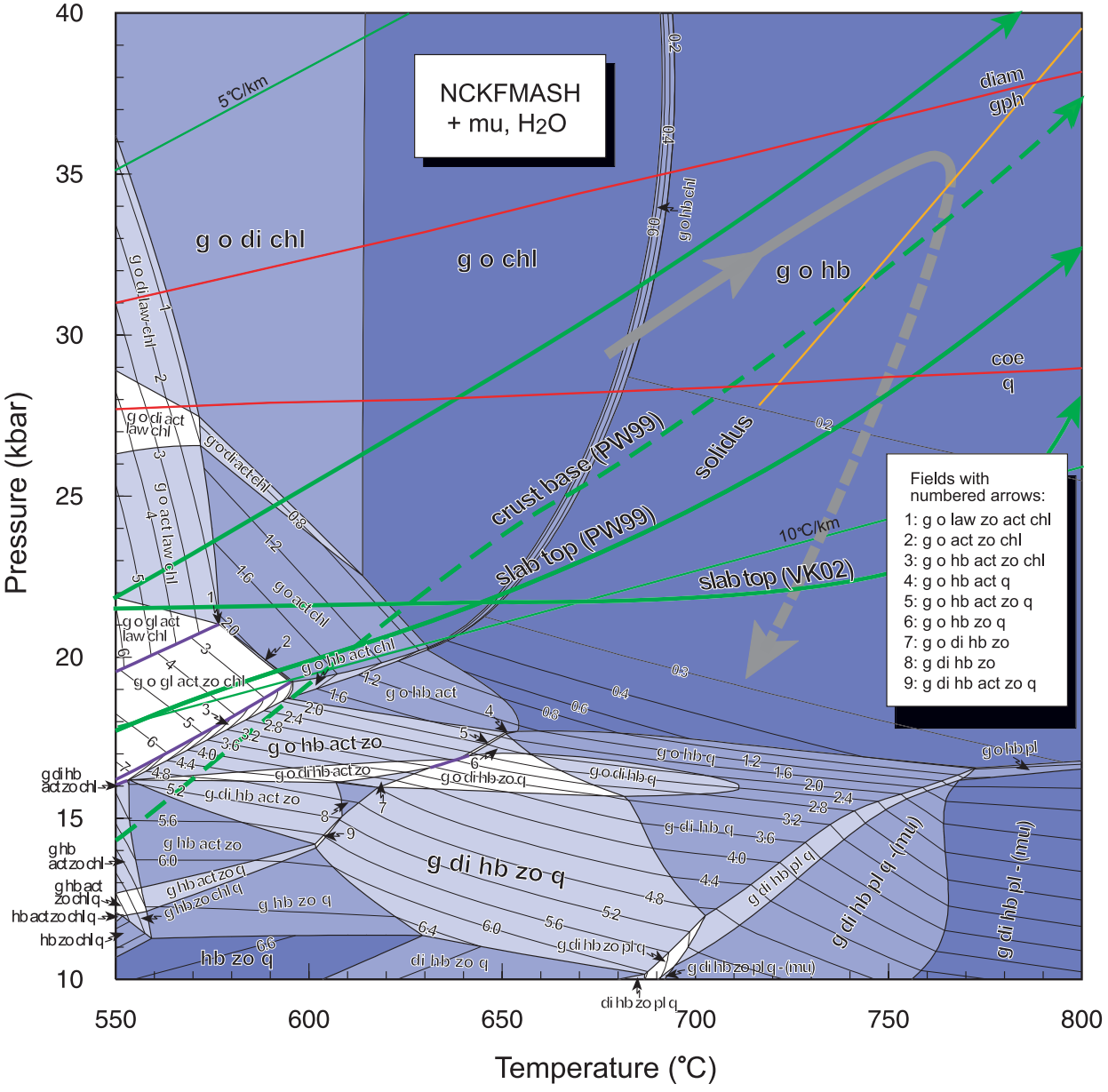

Fig. 10. *P–T* pseudosection of an Fe–Ti-rich eclogite (sample RL207) from Lanshantou in the Su-Lu terrane (Yang et al., 1998), contoured for H_2O content. Bulk composition of this sample is SiO_2 = 48·87, Al_2O_3 = 10·18, CaO = 13·58, MgO = 12·76, FeO = 11·85, K_2O = 0·01, Na_2O = 2·74, in mol %. This composition is typical of Fe–Ti-rich gabbros. The solidus for a phengite-bearing MORB composition is from Schmidt *et al.* (2004) (see text). *P–T* paths for model slabs are as in Fig. 9.

appears as a post-peak early retrograde mineral. Minor secondary quartz is observed in the matrix. Green amphibole, epidote, chlorite, and albite occur in veins.

A *P–T* pseudosection with H_2O in excess for this eclogite is presented in Fig. 10. It is rather different from that of the Mg–Al-rich eclogite. Lawsonite- and glaucophane-bearing assemblages are stable only at very low temperatures (<580°C and <600°C, respectively), and actinolite is again stable to higher pressure than glaucophane. The temperature stability of the three amphiboles is again hb > act > gl. The higher stability of chlorite reaches about 700°C at 40 kbar. The assemblage g + o + hb + mu is stable in a wide high *P–T* range. Plagioclase appears in assemblages at high-*T* and low-*P* conditions. Zoisite (epidote) is stable only at low *P–T* conditions. Kyanite and talc do not occur in rocks with such Fe-rich bulk compositions.

Calculated modes of minerals in the peak metamorphic assemblage of the eclogite are 51 mol % of garnet, 46 mol % of omphacite, 2·5 mol % of amphibole,

and 0·1 mol % of phengite (on a one-oxide basis). The calculated compositions of garnet and omphacite at 40 kbar and 760°C are $gr_{26}py_{27}alm_{47}$, and $Fe/(Fe + Mg)_o = 0{\cdot}16$ and $jd = Na/(Na + Ca) = 0{\cdot}53$, respectively, with garnet composition close to the analysed one ($gr_{26}py_{28}alm_{46}$). The calculated composition of omphacite is somewhat different from the analysed one [$Fe/(Fe + Mg)_o = 0{\cdot}20$ and $jd = 0{\cdot}40$]. The calculated composition of amphibole at the same P–T conditions is $Fe/(Fe + Mg)_{amp} = 0{\cdot}26$, $x(Al,M2) = 0{\cdot}62$, $x(Na,M4) = 0{\cdot}49$, $x(Na,A) = 1{\cdot}00$. Such an amphibole is not observed in the peak assemblage of the eclogite, and is compositionally different from the early retrograde amphibole, with $Fe/(Fe + Mg)_{amp} = 0{\cdot}2758$, $x(Al,M2) = 0{\cdot}5400$, $x(Na,M4) = 0{\cdot}3683$, $x(Na,A) = 0{\cdot}1740$). It is not clear whether the calculated presence of amphibole at peak conditions is flagging a shortcoming in the amphibole model used. On the other hand, because garnet and omphacite are homogeneous in composition, and mineral inclusions are only rarely observed, fractionation of the bulk composition during prograde metamorphism is not implied. Quartz is expected to appear in the rock matrix as pressure decreases (Fig. 10), in line with observations (Yang *et al.*, 1998). The secondary veins, however, cannot be explained by Fig. 10 because the bulk composition from which this local retrograde assemblage developed is clearly different from that of the whole-rock.

Several possible mechanisms have been proposed for the formation of q + ksp inclusions in eclogites, including trapping in omphacite either as solid inclusions during prograde metamorphism, when coesite/quartz was present, or as crystallized melt (Massonne, 1992; Yang *et al.*, 1998). According to Schmidt *et al.* (2004), muscovite in the assemblage g + o + mu + coe + H_2O starts to melt at about 750°C at 35 kbar in a bulk composition typical of mid-ocean ridge basalt (MORB), the solidus being a sextivariant to quinivariant boundary in the implied NCKFMASH pseudosection. Given the position of the solidus, the start of melting is inevitable in this rock with significant decompression. If H_2O is lost during melt crystallization, a melt inclusion isolated by omphacite could crystallize to coe/q + ksp + jd (in omphacite), accounting for the absence of phengite from the peak metamorphic assemblage and the presence of the q + ksp inclusions in omphacite.

Talc- and coesite-bearing zoisite-rich eclogite from Bixiling (Dabie terrane)

Zhang *et al.* (1995) described a talc- and coesite-bearing zoisite-rich eclogite (their sample 77I) at Bixiling in the Dabie terrane. The rock is composed of garnet, omphacite, zoisite (20–50 vol. %), quartz/coesite, talc, kyanite, rutile, actinolite, minor phengite, and chlorite. Coesite is reported to occur as inclusions in omphacite, kyanite, and also zoisite. Talc, replaced by actinolite, occurs both as minute inclusions in garnet, omphacite and zoisite, and as coarse grains in direct contact with these minerals. Based on these observations and also a P–T projection for end-member minerals, Zhang *et al.* (1995) argued that both talc and zoisite were UHP minerals in the eclogite.

A P–T pseudosection for the bulk composition of sample 77I in Zhang *et al.* (1995) is calculated (Fig. 11). Because neither H_2O nor loss-on-ignition was reported and the data were normalized to 100 wt %, H_2O is assumed here to be in excess. The labelling of clinopyroxenes is on the basis that the phase relations at the clinopyroxene solvus involves the more Na-rich clinopyroxene disappearing with increasing temperature. However, the clinopyroxene at peak conditions (labelled as di) can be reasonably called omphacite (see comparison of calculated and observed clinopyroxene compositions below). The diagram shows that g + di + zo + ky + coe form a stable assemblage at UHP conditions, explaining the preservation of coesite and its pseudomorphs in these minerals. However, talc is not stable in the stability field of coesite unless lawsonite is also present (and at temperatures <650°C; Fig. 11). Because lawsonite is not found either as mineral inclusions or anywhere in the rock, and talc does not share grain boundaries with coesite, talc crystallization was outside the stability field of lawsonite. In Fig. 11, talc in the absence of lawsonite appears in the divariant assemblage of o + di + zo + ta + q (+ g + mu + H_2O), which would account for its direct contact with garnet, clinopyroxene, and zoisite. As P–T increases, the talc-bearing assemblage is replaced by an assemblage of o + di + zo + ky (+ g + mu + H_2O), the talc inclusions in the other minerals being explained by prograde overgrowth. The coarse-grained talc in this eclogite, on the other hand, can be interpreted to be a retrograde mineral that crystallized in the same talc-bearing field. The replacement of talc by actinolite is well explained by further cooling and/or decompression from this field into actinolite-bearing ones (Fig. 11).

The calculated composition of the clinopyroxene within the stability field of the assemblage di + zo + ky + coe (+ g + mu + H_2O) at 31 kbar and 750°C is $jd = 0{\cdot}35$ and $Fe/(Fe + Mg)_o = 0{\cdot}06$, and that of garnet is $gr_{37}py_{36}alm_{27}$, fairly close to those reported by Zhang *et al.* (1995) for their omphacite [$jd = 0{\cdot}32$ and $Fe/(Fe + Mg)_o = 0{\cdot}06$] and garnet ($gr_{37}py_{31}alm_{32}$). The calculated modes of coesite (8·3 mol %), kyanite (1·6 mol %), and muscovite (<1 mol %) are in agreement with those reported by Zhang *et al.* (1995). However, the calculated mode of zoisite in the coesite stability field is <8 mol %, much lower than the reported 20–50 vol. %. None the less, the mode of zoisite increases as retrogression

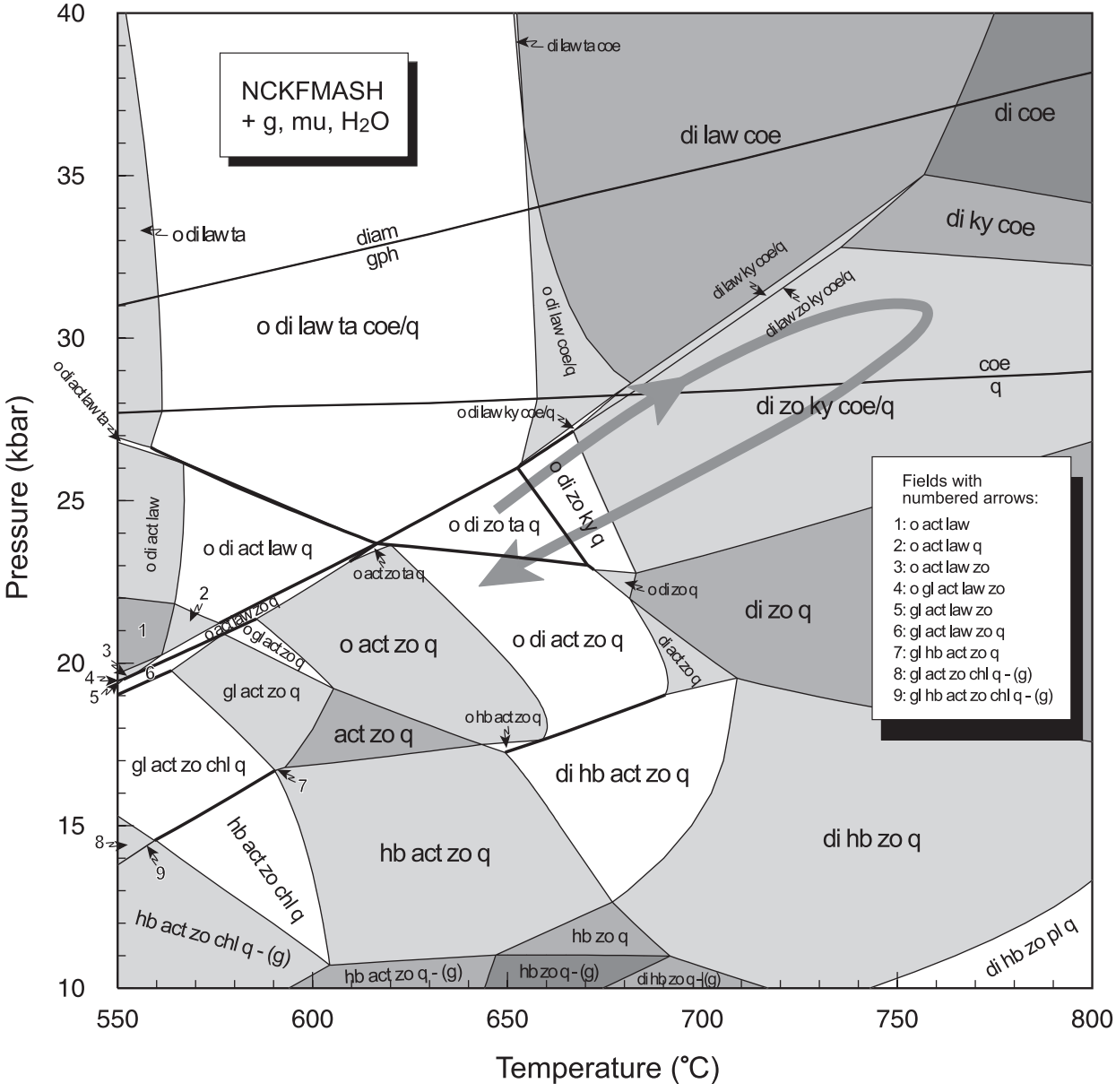

Fig. 11. *P–T* pseudosection of a talc- and coesite-bearing zoisite-rich eclogite from Bixiling in the Dabie terrane, described by Zhang *et al.* (1995). Bulk composition of this sample is $SiO_2 = 51{\cdot}7$, $Al_2O_3 = 10{\cdot}15$, CaO = 15·92, MgO = 14·44, FeO = 6·41, $K_2O = 0{\cdot}07$, $Na_2O = 1{\cdot}30$, in mol %. The thick grey line with arrows is the deduced *P-T* path for the eclogite (see text).

proceeds. For example, the mode of zoisite is 20 mol % at 22 kbar and 650°C (tip of the arrow head at the end of the *P–T* path in Fig. 11) in the divariant field of o + di + act + zo + q (+ g + mu + H_2O). The occurrence of chlorite and possible clinozoisite in some samples (Zhang *et al.*, 1995) implies further increase in the mode of epidote group minerals. Therefore it is reasonable to suppose that only a few per cent of zoisite was present at UHP conditions, and the rest crystallized during rehydration and retrogression.

UHP whiteschist from near Hualiangting reservoir (Dabie terrane)

A whiteschist is reported from near Hualiangting reservoir in the Dabie terrane (Rolfo *et al.*, 2000). The rock contains mainly quartz, with minor kyanite and talc. Omphacite is only found as inclusions in kyanite and epidote. A fine symplectite of amphibole + quartz + oligoclase, implying the previous presence of Na-bearing clinopyroxene, is also observed in the matrix. Kyanite and epidote are replaced by talc, and talc by actinolite.

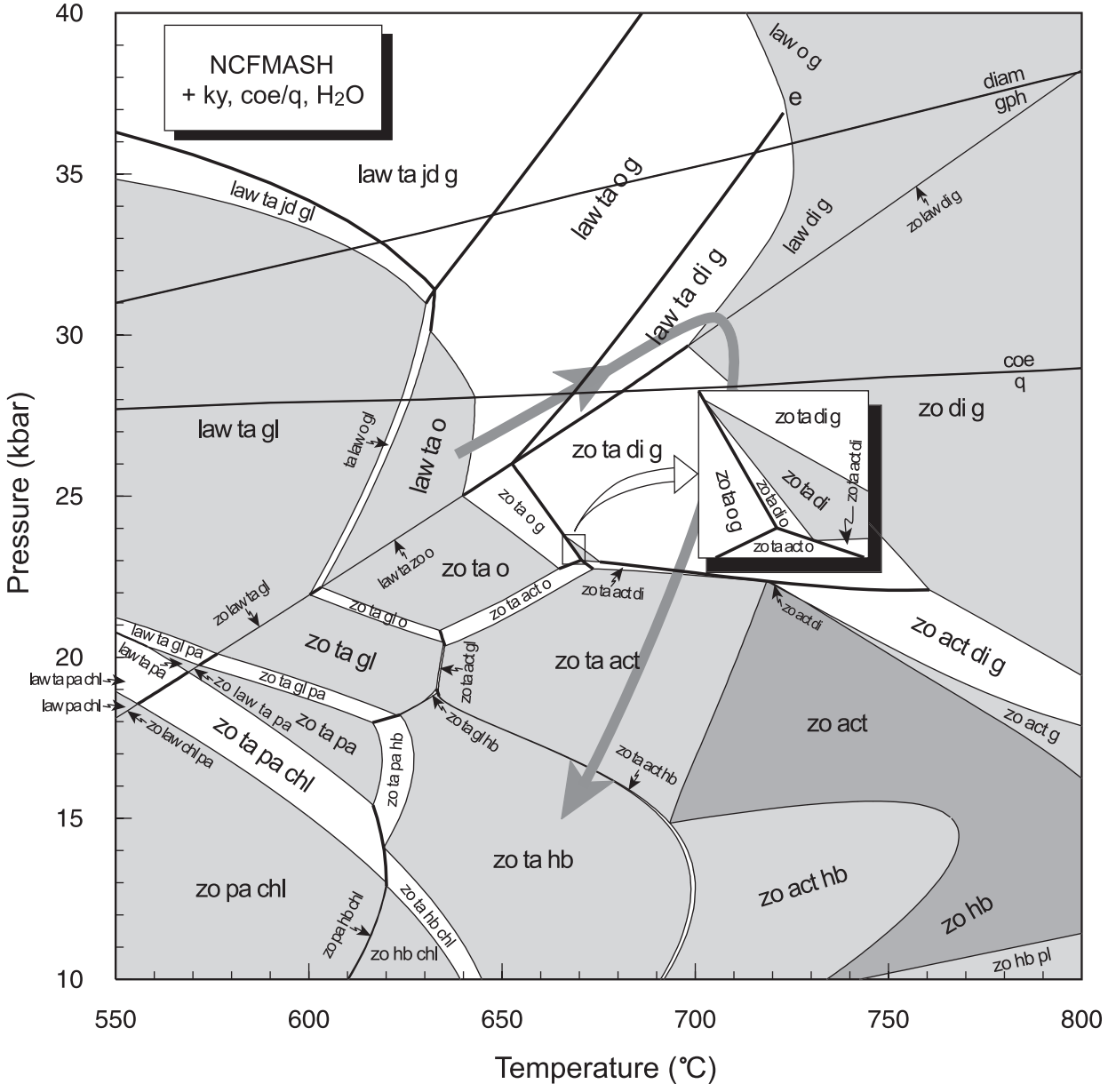

Fig. 12. *P–T* pseudosection of a whiteschist from Hualiangting in the Dabie terrane, described by Rolfo *et al.* (2000). Bulk composition used is SiO_2 = 85·24, Al_2O_3 = 6·84, CaO = 4·03, MgO = 3·63, FeO = 0·15, Na_2O = 0·11, in mol %. The inset shows an enlarged view of the rectangular area. The thick grey line is the deduced *P-T* path (see text).

Although the bulk composition of the whiteschist is reported, it is too low in Mg for the calculated pseudosection to have any talc in the *P–T* range possible for high-pressure rocks (>580 °C). The significant amount of Fe_2O_3 (1·34 wt %) in the reported bulk composition is relevant, but given that the present study is confined to a Fe^{3+}-free system, its role in the calculation of phase diagrams cannot be considered. Instead, a bulk composition is estimated for the whiteschist based on the petrographical description of Rolfo *et al.* (2000), ignoring the ferric iron in epidote. By assuming 70 mol % quartz, 8 mol % kyanite, 7 mol % talc, 12 mol % zoisite (representing epidote), 1 mol % omphacite, and 2 mol % amphibole, and using the reported mineral chemical data, the bulk composition is estimated to be SiO_2 = 85·24, Al_2O_3 = 6·84, CaO = 4·03, MgO = 3·63, FeO = 0·15, Na_2O = 0·11, on a mole basis, in the NCFMASH system. This composition is higher in Mg than the reported one but is closer to most other whiteschists (Schreyer, 1977).

The calculated P–T pseudosection with H_2O in excess (Fig. 12), explains the main features of this whiteschist. Because lawsonite is absent in the rock, only the assemblages of zo + di + g (+ ky + coe + H_2O) and zo + ta + di + g (+ ky + coe + H_2O), both appearing in the coesite stability field, may have been formed during peak metamorphism. However, because epidote is replaced by talc on retrogression, it is more reasonable to take zo + di + g to be the peak metamorphic assemblage. Therefore coesite, kyanite and diopside (jd <6 mol %) are the major minerals at this stage. The calculated mode of garnet is very low (<1 mol %); it can be either eliminated by retrogression or overlooked in observation. Because omphacite is described to occur as inclusions in kyanite and epidote, a prograde P–T path from the assemblage of either zo/law + ta + o + g (+ ky + q + H_2O) or zo/law + ta + o (+ ky + q + H_2O) to peak metamorphism is implied. The replacement of talc by actinolite can be explained by the appearance of zo + act + di (+ ky + q + H_2O) and zo + act (+ ky + q + H_2O) following zo + ta + di + g (+ ky + q + H_2O).

Dehydration of gabbroic rocks during deep subduction

The P–T pseudosections (Figs 9 and 10) for the Mg–Al-rich and Fe–Ti-rich gabbroic compositions are also contoured for H_2O content, the sum of the H_2O in the minerals under H_2O-saturated conditions. These are useful for considering closed-system behaviour of rocks (with fluid loss when it is generated) because rocks that are H_2O-saturated will remain H_2O-saturated while their P–T path crosses contours of decreasing value, but will tend to become fluid-absent when crossing contours of increasing value (see also Guiraud *et al.*, 2001). The suggestion is that preservation of mineral assemblages tends to occur from where a rock becomes fluid-absent. This assumption remains valid unless evidence for addition of fluid during prograde metamorphism is available. For the case of retrogression, ingress of external fluid is generally necessary, and additional phase diagrams considering fluid addition are needed to discuss retrogression.

The dehydration process is illustrated by considering the Mg–Al-rich and Fe–Ti-rich gabbroic compositions in relation to a P–T path intermediate between the 5°C/km and 10°C/km linear geotherms and cooler than geotherms for the slab–mantle interface (Peacock & Wang, 1999; Van Keken *et al.*, 2002; Figs 9 and 10). For these bulk compositions, chlorite and lawsonite are two important H_2O-carriers. Amphibole may or may not be a major H_2O-carrier to depth. Dehydration in eclogites solely as a result of amphibole breakdown will not be common. The Mg–Al-rich eclogite following such a P–T path releases about 4 mol % of H_2O from 550°C and 22 kbar to 590°C and 24·5 kbar, as a result of dehydration of actinolite, chlorite, and lawsonite (Fig. 9). When the univariant reaction chl + act + law = o + di + g + ta + H_2O is crossed, actinolite breaks down completely, and talc appears in the new divariant assemblage. When the mineral assemblage changes from the divariant g + o + di + law + ta + chl (+ mu + H_2O) to the trivariant g + o + di + law + ta (+ mu + H_2O), chlorite breaks down completely. With increasing P–T the rock in the trivariant field ceases to dehydrate and even rehydrates slightly (if a H_2O source is available) (Fig. 9). When entering the g + o + di + law + ta + coe (+ mu + H_2O) divariant field, the rock dehydrates quickly from about 7·0 mol % to about 5·4 mol %. Then talc breaks down completely, and the rock dehydrates at a lower rate in the trivariant field g + o + di + law + coe (+ mu + H_2O). When the rock is heated to above the temperature of the top of the solvus for omphacite and diopside, its dehydration rate becomes higher again in the quadrivariant field of g + o + law + coe (+ mu + H_2O), until lawsonite breaks down completely. This eclogite composition ceases to dehydrate at this point along this relatively warm slab geotherm (Fig. 9), with phengite being the only K-bearing mineral and no metamorphic reaction causing it to break down in this high P–T range.

In contrast to the Mg–Al-rich gabbroic composition, dehydration in the more Fe-rich composition is effectively complete at much lower P–T conditions under equivalent conditions. This is because the P–T field involving primarily garnet + omphacite extends to lower T for more Fe-rich rock compositions. At >600°C, the Fe-rich eclogite will contain little chlorite. The amount of phengite depends on the K content; in this case H_2O sums to less than 0·8 mol %. UHP metamorphism of this composition therefore produces an essentially anhydrous mineral assemblage (Fig. 10).

These results show that whether or not a univariant dehydration reaction takes place is strongly dependent on bulk composition. In most cases, dehydration takes place continuously, with H_2O content controlled by divariant or higher variance assemblages (Figs 12 and 13), rather than abruptly, as predicted by using intersection of univariant dehydration reactions in P–T projections with geotherms in various types of subducting slab (Delany & Helgeson, 1978; Hacker *et al.*, 2003*a*, 2003*b*). Therefore, under H_2O-saturated conditions, fluid fluxes in subduction zones may be continuous (see also Schmidt & Poli, 1998; Kerrick & Connolly, 2001), with the rate of dehydration being a function of pressure and temperature.

Mineral assemblages may or may not dehydrate during subduction and also exhumation, depending on the relative slopes of H_2O-content contours in P–T

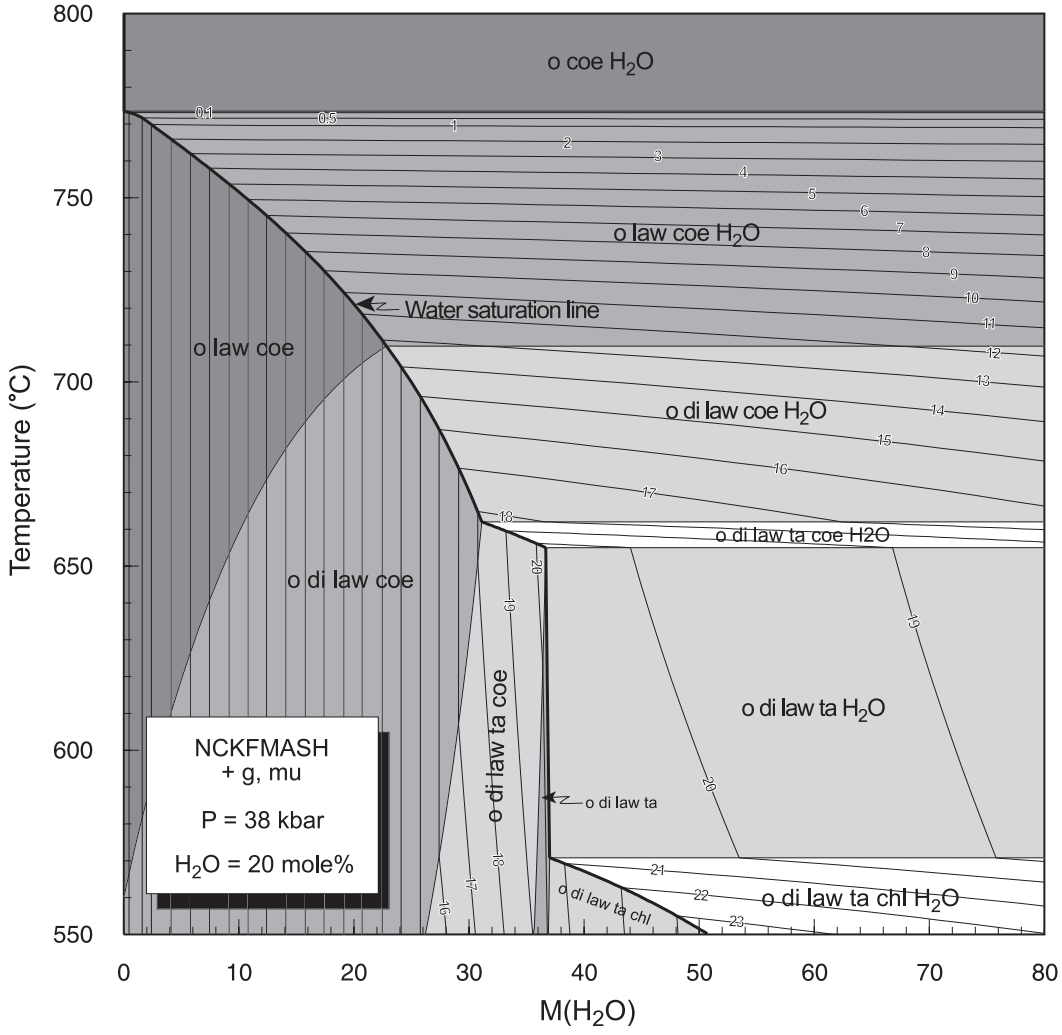

Fig. 13. T–$M(H_2O)$ pseudosection at 38 kbar for the Mg–Al-rich eclogite (sample SL01) in Fig. 9. $M(H_2O)$ is the percentage of H_2O in the system. $M(H_2O) = 0$ corresponds to the bulk composition on an anhydrous basis, and moving to the right on the diagram involves adding an increasing percentage of H_2O to this composition.

pseudosections and the P–T path being followed (Guiraud *et al.*, 2001). For example, when the Mg–Al-rich eclogite is heated and compressed into the trivariant field of g + o + di + law + ta (+ mu + H_2O) (Fig. 9), it ceases to dehydrate and becomes H_2O undersaturated (if no external H_2O source is available), because further heating and compression requires hydration for Fig. 9 to remain applicable. Water saturation is re-established in the divariant field of g + o + di + law + ta + coe (+ mu + H_2O). For a P–T path crossing the trivariant field, chlorite breaks down and the assemblage g + o + di + law + ta (+ mu + H_2O) is formed at the boundary of the chlorite-bearing divariant field, but no reaction takes place afterwards within this field because no H_2O is available. Therefore, the trivariant assemblage is likely to be preserved until the rock enters the divariant field of g + o + di + law + ta + coe (+ mu + H_2O), where H_2O required for equilibration is available and reaction is activated. It is therefore possible that low P–T minerals can be preserved in minerals growing at high P–T conditions.

If H_2O is released during peak metamorphism and lost from the rock, the high P–T mineral assemblages are likely to be preserved during exhumation, regardless of the rate of exhumation. However, when the retrograde P–T path crosses a mineral assemblage field with decreasing values of H_2O content contours, for example the transformation from eclogite facies into granulite facies when entering the divariant field of g + di + zo + hb + pl + q in the lower left part of Fig. 9, the eclogite dehydrates as a result of the breakdown of zoisite. In such a case, the eclogite assemblage may not be

preserved. This also has important implications for fluid flow in subduction zones: exhumation of eclogites not only absorbs water, but can also release it, depending on bulk composition and P–T path.

DISCUSSION

The P–T projections provide an appropriate framework for the construction of the pseudosections for considering the metamorphic histories of some UHP eclogites and a whiteschist. The P–T pseudosections for the eclogites used as examples have proved useful in the interpretation of observations related to UHP metamorphism, and also predict behaviour of mineral assemblages in deeply subducted rocks. However, other factors, such as varying fluid composition, oxidation state, additional components (such as Ti, Mn, etc.) and phases (such as rutile, ilmenite, sphene and partial melt), will need to be taken into account in the future, as the appropriate thermodynamic models become available. For example, the wide high variance field in the high P–T range of Fe-rich eclogites (Fig. 10) may be subdivided once rutile, ilmenite and sphene are incorporated in the modelling.

The role of ferric iron becomes important for more oxidized rocks. Whereas the substitution of ferric iron in epidote and garnet can already be handled, and there is the beginning of a model for amphiboles in Dale *et al.* (2005), there is no model yet for clinopyroxene. In addition, such substitutions are critical with regard to improving Fe^{2+}–Mg exchange thermometry between garnet and omphacite (Štípská & Powell, 2005). The presence of ferric iron may reduce the miscibility gaps between diopside, omphacite, and jadeite, and between actinolite, hornblende, and glaucophane. This may be the reason why equilibrium coexistence of the clinopyroxenes is only rarely observed (Tsujimori *et al.*, 2005).

It is worthwhile noting that chlorite inclusions are commonly found in eclogite zircon and/or garnet in the UHP eclogites from the NQM and Su-Lu–Dabie terranes in China. This indicates that chlorite dehydration may have been an important source for fluids in these subduction zones. On the other hand, evidence for the possible presence of lawsonite is only rarely observed. For the eclogite examples used here, no evidence is available to suggest that they experienced metamorphism in the stability field of lawsonite.

Given that it is this absence of lawsonite that is a central piece of evidence used in deducing prograde P–T paths for the UHP eclogites, it is necessary to establish what controls lawsonite stability. The lawsonite breakdown reaction is a dehydration reaction in the CASH subsystem, law = zo + ky + q + H_2O, so anything that affects $a(H_2O)$ will affect lawsonite stability, and that is considered next. However, even if this limit is displaced down temperature as seems likely by a relatively small amount, the limit sits at the warmer end of the range of geotherms suggested for subduction. A conjecture might be that the UHP eclogites that are exhumed are associated with such warmer geotherms.

There are two ways in which the assumption of $a(H_2O) = 1$ may be varied: one is to consider fluid-absent conditions, the other is to have fluid-present but to have $a(H_2O) < 1$, as a result of the fluid being solute-rich, possibly also including CO_2. Figure 13 is a diagram showing the dependence of mineral assemblage on temperature and the per cent of H_2O in a bulk composition, a so-called T–$M(H_2O)$ pseudosection, for the eclogite sample SL01 at 38 kbar, contoured for the mode of lawsonite. A discussion of $M(H_2O)$, as well as $a(H_2O)$, has been given by Powell *et al.* (2005). Under fluid-present conditions, the amount of lawsonite decreases with increasing temperature. Under fluid-absent conditions, the amount of water in the bulk composition has no effect on lawsonite stability, although its mode decreases with water content (Fig. 13).

Alternatively, the P–T path was not so warm but the above phase relations calculated by assuming $a(H_2O) = 1$ are at temperatures that are too high at a particular pressure, but that $a(H_2O)$ was significantly less than unity. The latter situation is plausible, given the increasing solubility of silicates, oxides, carbonates, sulphate/sulphides, chloride, etc. in H_2O at high pressure (Philippot & Rumble, 2000; Touret, 2001; Ferrando *et al.*, 2005). To emulate the effect of the fluid being solute-rich, the consequent reduction of $a(H_2O)$ can be seen on the T–$a(H_2O)$ pseudosection calculated at 38 kbar (Fig. 14). The diagram shows that all the boundaries between mineral assemblages shift to lower temperature when the hydrous fluid in equilibrium with the eclogite minerals is solute-rich. The upper temperature stability of lawsonite in this eclogite is reduced by more than 100°C when $a(H_2O)$ is reduced to 0·5, noting that this is a likely upper limit for the reduction at UHP conditions, and an overestimate at the HP conditions in which lawsonite would already be stable. However, it is clear that water activity needs to be constrained before a P–T path followed by an eclogite can be more precisely constrained. Sufficiently precise thermometry not dependent on $a(H_2O)$ would help to resolve this issue.

Partial melting at high P–T is not considered in the calculations, because of the lack of an appropriate thermodynamic model for melt at high pressure. It is evident, however, that eclogites can experience partial melting, especially involving phengite at UHP conditions. A melt model will have to be included in modelling such UHP crustal rocks in order to better understand deep processes in subducting slabs.

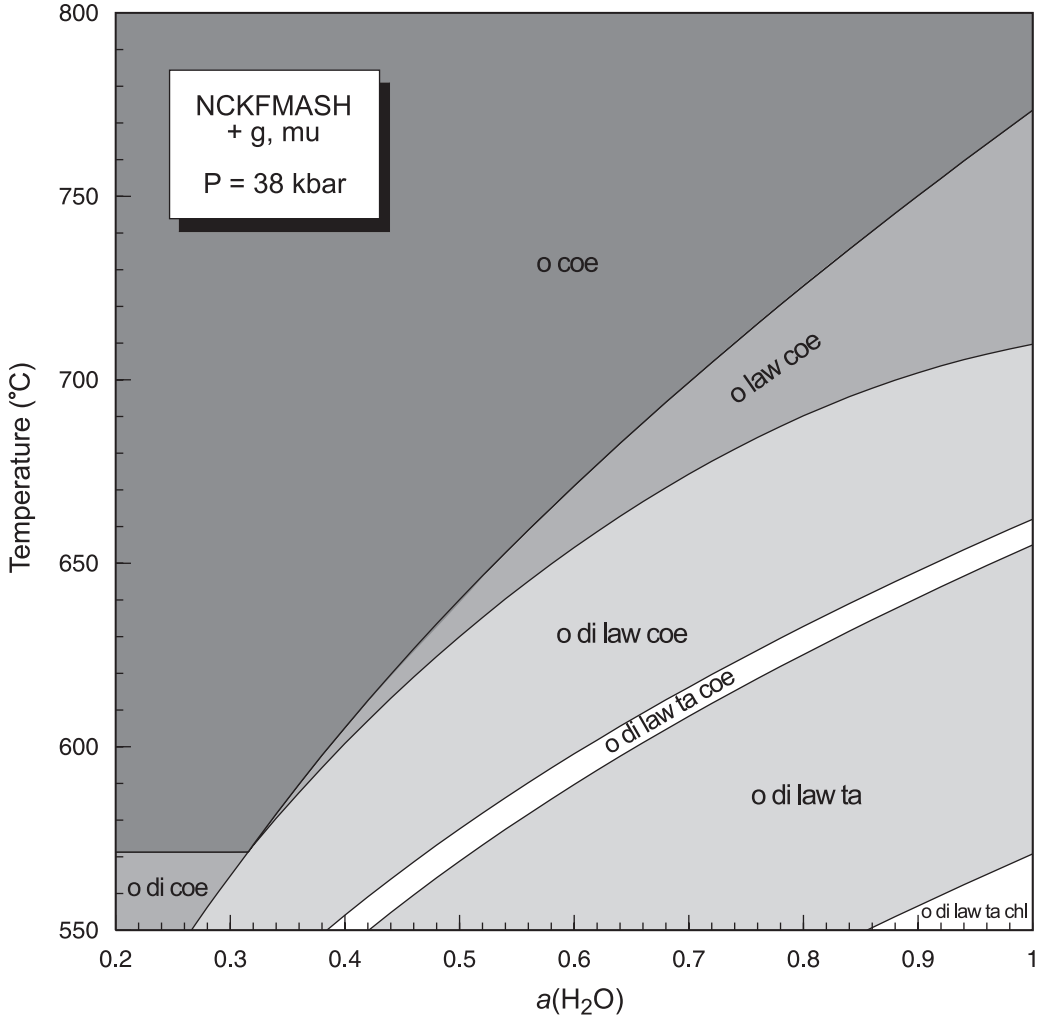

Fig. 14. T–$a(H_2O)$ pseudosection at 38 kbar for the Mg–Al-rich eclogite (sample SL01) in Fig. 9.

Eclogite dehydration and the origin of UHP eclogites and whiteschists may be discussed in the context of modelled slab geotherms. With the progression from simpler rheological models for the mantle wedge (e.g. Peacock & Wang, 1999), to a temperature- and stress-dependent model (e.g. Van Keken *et al.*, 2002), the within-slab temperature profile steepens as the corner flow in the mantle wedge is stronger and therefore much more effective at heating the slab top (compare the slab-top temperatures in Figs 9 and 10). Combining the effect of depth in the slab with the effect of the age of the subducted slab and the rate of subduction, a very wide range of possible P–T paths for subducted rocks is implied, extending down below 400°C for the crust base. In this range, and given the uncertainties in the modelling, it is possible to suggest that the P–T paths for the rocks in Figs 9–12 correspond to relatively hot geotherms.

CONCLUSIONS

(1) With increasing pressure and temperature, the number of univariant and invariant reactions in the system NCKFMASH P–T grid decreases, only one invariant point and associated univariant reactions appear in the UHP range, and no reaction appears in the high P–T range, except for the degenerate reaction law = zo (Fig. 5). However, there are several invariant points and associated univariant reactions appearing in the UHP range of the subsystem P–T grids. These subsystem reactions provide useful information about the high-variance assemblages in the full system at UHP conditions.

(2) UHP mineral assemblages, and in some cases also mineral chemistry, match the phase relationships calculated with THERMOCALC. The dependence of phase relationships on bulk composition as well as on P–T is demonstrated by the pseudosections.

(3) Water content contours on P–T pseudosections provide information concerning dehydration/hydration during subduction of UHP rocks. For the examples used here chlorite and lawsonite are the two main H_2O-carriers. Water contents in divariant or higher variance assemblages decrease with increasing temperature, and dehydration takes place gradually across such fields. Therefore, fluid fluxes in subduction zones for the warm slab conditions responsible for UHP rocks are likely to be continuous.

ACKNOWLEDGEMENTS

J.-J.Y. acknowledges financial support by the Natural Science Foundation of China (Nos 40473022 and 40421202). He is also grateful to Chunjing Wei for assistance. R.P. thanks the Australian Research Council for continuing support with ARC DP0209461 and DP0451770.

SUPPLEMENTARY DATA

Supplementary data for this paper are available at *Journal of Petrology* online.

REFERENCES

Carson, C. J., Powell, R. & Clarke, G. C. (1999). Calculated mineral equilibria for eclogites in CaO–Na_2O–FeO–MgO–Al_2O_3–SiO_2–H_2O: application to the Pouébo Terrane, Pam Peninsula, New Caledonia. *Journal of Metamorphic Geology* **17**, 9–24.

Chopin, C. (2003). Ultrahigh-pressure metamorphism: tracing continental crust into the mantle. *Earth and Planetary Science Letters* **212**, 1–14.

Chopin, C. & Sobolev, N. V. (1995). Principal mineralogic indicators of UHP in crustal rocks. In: Coleman, R. G. & Wang, X. (eds) *Ultrahigh Pressure Metamorphism*. Cambridge: Cambridge University Press, pp. 96–131.

Coggon, R. & Holland, T. J. B. (2002). Mixing properties of phengitic micas and revised garnet–phengite thermobarometers. *Journal of Metamorphic Geology* **20**, 683–696.

Dale, J., Holland, T. J. B. & Powell, R. (2000). Hornblende-garnet-plagioclase thermobarometry: a natural assemblage calibration of the thermodynamics of hornblende. *Contributions to Mineralogy and Petrology* **140**, 353–362.

Dale, J., Powell, R., White, R. W., Elmer, F. L. & Holland, T. J. B. (2005). A thermodynamic model for Ca–Na clinoamphiboles in Na_2O–CaO–FeO–MgO–Al_2O_3–SiO_2–H_2O–O for petrological calculations. *Journal of Metamorphic Geology* **23**, 771–791.

Delany, J. M. & Helgeson, H. C. (1978). Calculation of the thermodynamic consequences of dehydration in subducting ocean crust to 100 kb and >800°C. *American Journal of Science* **278**, 638–686.

Ferrando, S., Frezzotti, M. L., Dallai, L. & Compagnoni, R. (2005). Multiphase solid inclusions in UHP rocks (Su-Lu, China): remnants of supercritical silicate-rich aqueous fluids released during continental subduction. *Chemical Geology* **223**, 68–81.

Guiraud, M., Holland, T. J. B. & Powell, R. (1990). Calculated mineral equilibria in the greenschist–blueschist–eclogite facies in Na_2O–FeO–MgO–Al_2O_3–SiO_2–H_2O. *Contributions to Mineralogy and Petrology* **104**, 85–98.

Guiraud, M., Powell, R. & Rebay, G. (2001). H_2O in metamorphism and unexpected behaviour in the preservation of metamorphic mineral assemblages. *Journal of Metamorphic Geology* **19**, 445–454.

Hacker, B. R., Abers, G. A. & Peacock, S. M. (2003*a*). Subduction factory 1. Theoretical mineralogy, densities, seismic wave speeds, and H_2O contents. *Journal of Geophysical Research* **108**, 2029.

Hacker, B. R., Peacock, S. M., Abers, G. A. & Holloway, S. D. (2003*b*). Subduction factory 2. Are intermediate-depth earthquakes in subducting slabs linked to metamorphic dehydration reactions? *Journal of Geophysical Research* **108**, 2030.

Harley, S. L. & Carswell, D. A. (1995). Ultradeep crustal metamorphism: a prospective review. *Journal of Geophysical Research* **100**, 8367–8380.

Holland, T. J. B., Baker, J. & Powell, R. (1998). Mixing properties and activity-composition relationships of chlorites in the system MgO-FeO-Al_2O_3-SiO_2-H_2O. *European Journal of Mineralogy* **10**, 395–406.

Holland, T. J. B. & Powell, R. (1996). Thermodynamics of order–disorder in minerals. 2: symmetric formalism applied to solid solutions. *American Mineralogist* **81**, 1425–1437.

Holland, T. J. B. & Powell, R. (1998). An internally consistent thermodynamic dataset for phases of petrological interest. *Journal of Metamorphic Geology* **16**, 309–343.

Holland, T. J. B. & Powell, R. (2003). Activity–composition relations for phases in petrological calculations: an asymmetric multicomponent formulation. *Contributions to Mineralogy and Petrology* **145**, 492–501.

Kerrick, D. M. & Connolly, J. A. D. (2001). Metamorphic devolatilization of subducted oceanic metabasalts: implications for seismicity, arc magmatism and volatile recycling. *Earth and Planetary Science Letters* **189**, 19–29.

Krogh Ravna, E. J. & Terry, M. P. (2004). Geothermobarometry of UHP and HP eclogites and schists—an evaluation of equilibria among garnet–clinopyroxene–kyanite–phengite–coesite/quartz. *Journal of Metamorphic Geology* **22**, 579–592.

Marmo, B. A., Clarke, G. L. & Powell, R. (2002). Fractionation of bulk rock composition due to porphyroblast growth: effects on eclogite facies mineral equilibria, Pam Peninsula, New Caledonia. *Journal of Metamorphic Geololgy* **20**, 151–165.

Massonne, H.-J. (1992). Thermodynamical determination of water-activities relevant to eclogitic rocks. In: Kharaka, Y. K. & Maest, A. S. (eds) *Water–Rock Interaction*. Rotterdam: Bakkerman, pp. 1523–1526.

Massonne, H.-J. (1995). Experimental and petrogenetic study of UHPM. In: Coleman, R. G. & Wang, X. (eds) *Ultrahigh Pressure Metamorphism*. Cambridge: Cambridge University Press, pp. 33–95.

Massonne, H.-J. & Schreyer, W. (1989). Stability field of the high-pressure assemblage talc + phengite and two new phengite barometers. *European Journal of Mineralogy* **1**, 391–410.

Peacock, S. M. & Wang, K. (1999). Seismic consequences of warm versus cool subduction metamorphism: examples from southwest and northeast Japan. *Science* **286**, 937–939.

Philippot, P. & Rumble, D. (2000). Fluid–rock interactions during high-pressure and ultrahigh-pressure metamorphism. *International Geology Review* **42**, 312–327.

Poli, S. & Schmidt, M. W. (1998). The high-pressure stability of zoisite and phase relationships of zoisite-bearing assembalges. *Contributions to Mineralogy and Petrology* **130**, 162–175.

Powell, R., Holland, T. J. B. & Worley, B. (1998). Calculating phase diagrams involving solid solutions via non-linear equations, with examples using THERMOCALC. *Journal of Metamorphic Geology* **16**, 577–588.

Powell, R. & Holland, T. J. B. (1999). Relating formulations of the thermodynamics of mineral solid solutions: activity modeling of pyroxenes, amphiboles, and micas. *American Mineralogist* **84**, 1–14.

Powell, R., Guiraud, M. & White, R. W. (2005). Truth and beauty in metamorphic phase-equilibria: conjugate variables and phase diagrams. *Canadian Mineralogist* **43**, 21–33.

Powell, R. & Sandiford, M. (1988). Sapphirine and spinel phase relationships in the system FeO-MgO-Al_2O_3-SiO_2-TiO_2-O_2 in the presence of quartz and hypersthene. *Contributions to Mineralogy and Petrology* **98**, 64–71.

Rebay, G. & Powell, R. (2002). The formation of eclogite facies metatroctolites and a general petrogenetic grid in Na_2O–CaO–FeO–MgO–Al_2O_3–SiO_2–H_2O (NCFMASH). *Journal of Metamorphic Geology* **20**, 813–826.

Rolfo, F., Compagnoni, R., Xu, S. & Jiang, L. (2000). First report of felsic whiteschist in the ultrahigh-pressure metamorphic belt of Dabie Shan, China. *European Journal of Mineralogy* **12**, 883–898.

Schmidt, M. W. & Poli, S. (1998). Experimentally based water budgets for dehydrating slabs and consequences for arc magma generation. *Earth and Planetary Science Letters* **163**, 361–379.

Schmidt, M. W., Vielzeuf, D. & Auzanneau, E. (2004). Melting and dissolution of subducting crust at high pressures: the key role of white mica. *Earth and Planetary Science Letters* **228**, 65–84.

Schreyer, W. (1977). Whiteschists: their compositions and pressure–temperature regimes based on experimental, field, and petrographic evidence. *Tectonophysics* **43**, 127–144.

Song, S., Yang, J. S., Xu, Z. Q., Liou, J. G. & Shi, R. D. (2003). Metamorphic evolution of the coesite-bearing ultrahigh-pressure terrane in the North Qaidam, Northern Tibet, NW China. *Journal of Metamorphic Geology* **21**, 631–644.

Štípská, P. & Powell, R. (2005). Constraining the *P–T* path of a MORB-type eclogite using pseudosections, garnet zoning and garnet–clinopyroxene thermometry: an example from the Bohemian massif. *Journal of Metamorphic Geology* **23**, 725–743.

Touret, J. L. R. (2001). Fluids in metamorphic rocks. *Lithos* **55**, 1–25.

Tsujimori, T., Liou, J. G. & Coleman, R. G. (2005). Coexisting retrograde jadeite and omphacite in a jadeite-bearing lawsonite eclogite from the Motagua fault zone, Guatemala. *American Mineralogist* **90**, 836–842.

Van Keken, P. E., Kiefer, B. & Peacock, S. M. (2002). High-resolution models of subduction zones: implications for mineral dehydration reactions and the transport of water into the deep mantle. *Geochemistry, Geophysics, Geosystems* **3**, 1056, doi:10.1029/2001GC000256.

Wei, C. & Powell, R. (2006). Calculated phase relations in the system NCKFMASH (Na_2O–CaO–K_2O–FeO–MgO–Al_2O_3–SiO_2–H_2O) for high-pressure metapelites. *Journal of Petrology* **47**, 385–408.

Wei, C. J., Powell, R. & Zhang, L. F. (2003). Eclogites from the south Tianshan, NW China: petrological characteristic and calculated mineral equilibria in the Na_2O–CaO–FeO–MgO–Al_2O_3–SiO_2–H_2O system. *Journal of Metamorphic Geology* **21**, 163–179.

Yang, J.-J. & Deng, J.-F. (1994). Garnet peridotites and eclogites in the northern Qaidam Mountains, Tibetan plateau: a first record. In: Ernst, W. G. & Liou, J. G. (eds) *First Workshop on UHP Metamorphism and Tectonics*. Stanford, CA: ILP Task Group III-6, Stanford University, p. A-20.

Yang, J.-J., Godard, G. & Smith, D. C. (1998). K-feldspar in the coesite pseudomorphs in an eclogite from Lanshantou (Eastern China). *European Journal of Mineralogy* **10**, 969–985.

Zhang, R. Y., Liou, J. G. & Cong, B. (1995). Talc-, magnesite-, and Ti-clinohumite-bearing ultrahigh-pressure meta-mafic and ultramafic complex in the Dabie Mountains, China. *Journal of Petrology* **36**, 1011–1037.